Control Algorithm Design for High-Quality Self ServoWriting (SSW) Process in HDDs

Nancy Dong , Graduate Student Researcher

Masayoshi Tomizuka , Professor

Department of Mechanical Engineering

University of California at Berkeley, California

ABSTARCT

Self ServoWriting (SSW) is an attractive method for writing servo information on hard disks because it significantly saves the manufacturing cost and maintains the servowriting quality. Before SSW process, the servo writer prepares each HDD unit by writing either concentric seed tracks or spiral reference tracks. This report presents several control algorithms for SSW based on concentric seed tracks. During SSW, the recording heads must be controlled in both radial and tangential directions of rotating disks.

Section 2 discusses position error compensation for SSW process in the radial direction. Two novel control algorithms are proposed: Iterative Learning Control (ILC) and Two-Dimensional (2-D) control. An ILC structure is designed by learning the previous-track position errors in order to contain the Radial Error Propagation (REP) in the position control loop. SSW process is also modeled as a 2-D Roesser Model (2-D RM). The 2-D RM allows us to employ powerful tools offered by 2-D system theory. The conditions for asymptotic convergence and monotonic convergence are analyzed in both control schemes. An L_1 optimization problem is formulated to obtain the controller parameters.

In section 3, timing error compensation for SSW process in the tangential direction is studied. In order to contain the closure error in each track and attenuate the timing error propagation from track to track in the timing control loop, an Adaptive Feedforward Compensation (AFC) scheme is proposed and an adaptive filter is designed by applying the Filtered-X Least Mean Square (FXLMS) algorithm.

Conclusions and challenges for future research are given in section 4.

CONTENTS

LISTS OF FIGURES

1 INTRODUCTION

1.1 Servo Writing Process

Servowriting is a manufacturing process where the data tracks and servo sectors (as shown in Figure 1.1) are defined on the disk platters by writing the servo patterns, which are used to measure the head position relative the track centerline and generate the feedback signal during read and write operation. There are several conventional methods used to write the servo patterns. The common one is to write the position (servo burst) and timing (synchronization mark) information onto the disk surface by using an external laser-guided push-pin mechanism. This costly servo writer accurately move the HDD actuator so that the write head is positioned on the desired tracks.

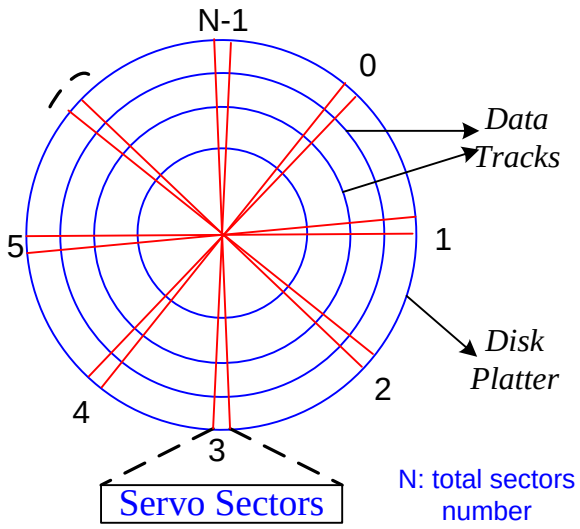

Figure 1.1 Data Tracks and Servo Sectors on a Disk Platter

The conventional servowriting method has some disadvantages. It needs expensive external devices for positioning the write head to write the servo patterns and requires clean room environment not to contaminate the disk drive interior. Furthermore, frequent calibrations may be required. The conventional method faces progressively difficult challenges as the Track Per Inch (TPI) continues increasing in the industry. These challenges come from different factors. Firstly, conventional servowriting requires several revolutions of the spindle to create one servo track. Therefore, the total time required for servowriting an HDD unit increases, i.e., the throughput increases, proportionately as the number of tracks per surface increases. This decrease in

the throughput of servowriting requires more servo writers to meet the production target. This, in turn, requires a more floor space in the clean room. Secondly, for smaller drives, the jigs and fixtures for servowriting become smaller. It is challenging to design the push-pin mechanism that is small and yet sufficiently stiff.

Self ServoWriting (SSW) is an alternative method of writing servo patterns to satisfy the demand for higher throughput without increasing the production cost and process time.

SSW has been attractive in HDD industry because it not only potentially saves the manufacturing cost and operation time, but also effectively maintains the servowriting quality. This process can be performed outside expensive clean room. During SSW, the timing (tangential) and position (radial) information are regenerated from the previously written track by using the existing head of HDD. Hence, the external servo writers are no longer needed and servowriting does not have to be processed in the clean room environment. The process of SSW is shown in Figure 1.2 and it generally contains the following steps:

(1) A seed track which may be written by a servo writer is available on the disk. Position Error Signal (PES) is obtained when the read head is track-following on the seed track.

(2) Assume a constant read-head-to-write-head offset of one track width. Make the read head to follow the seed track in the usual track following mode while the write head writes the servo patterns for the next track.

(3) The read head uses the newly written track as a following reference while the write head writes the next track.

(4) Repeat step (3) until all tracks are written.

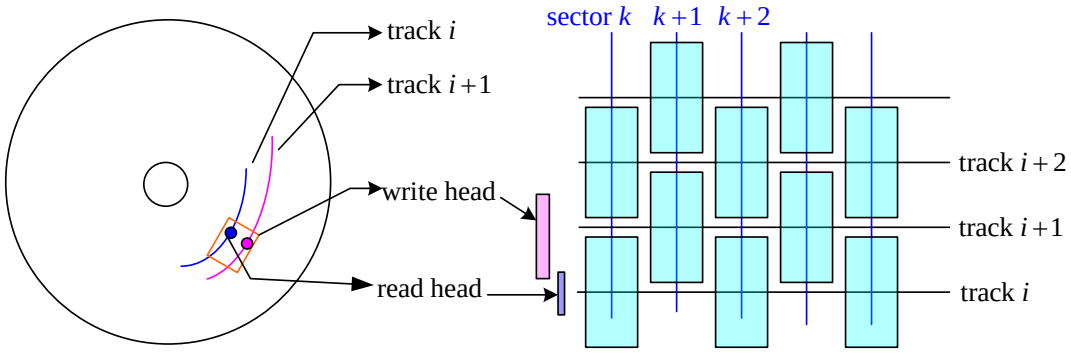

Figure 1.2 Illustration of SSW Process

1.2 Servo System in SSW Process

The servo system in SSW involves two control loops as shown in Figure 1.3: position control loop and timing control loop. In the position control loop, a Voice Coil Motor (VCM) is controlled to maintain the heads over the target track centerline during reading and writing operations. And in the timing control loop, a Phase Lock Loop (PLL) is generally used to generate the servo writing clock signal.

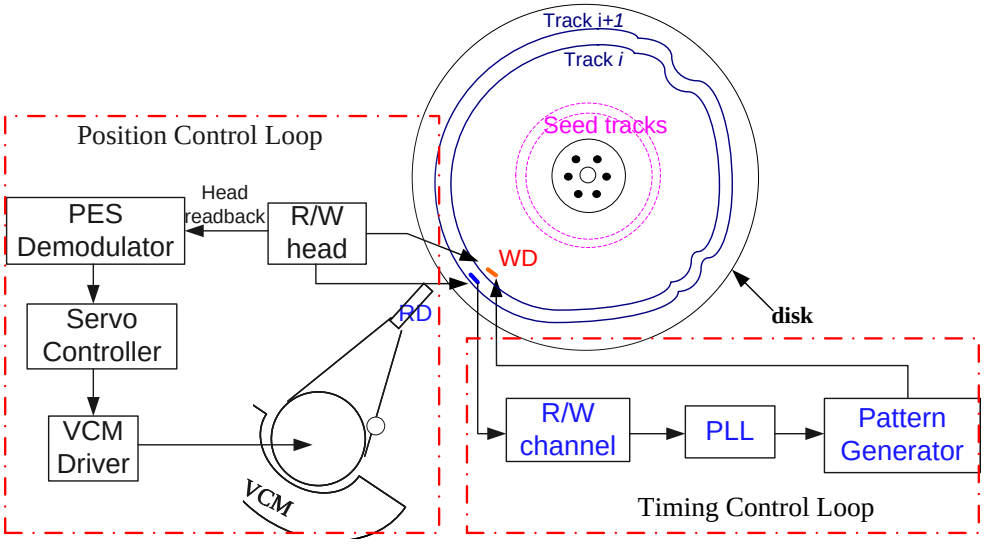

Figure 1.3 Block Diagram for SSW Servo System

1.3 Control Problems in SSW Servo System

Figure 1.4 illustrates the errors occurring on the disk during SSW process. In the position control loop, some position errors along radial direction cause the noncircuity of servo tracks. In the timing control loop, certain timing errors in circumferential direction result in 'warping' of the servo sectors on the disk.

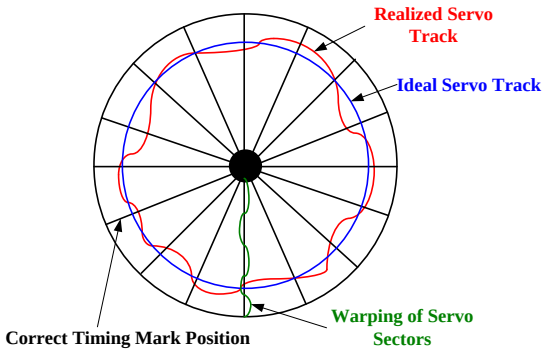

Figure 1.4 Errors on the Disk

Therefore, there are two critical control problems in SSW process:

(1) All the servo tracks should ideally be concentric. If not so, the data tracks will be squeezed, resulting in AC track squeeze. In the position control loop, the position of the write head with respect to the track centerline is controlled by controlling the VCM. Any disturbance and eccentricity present during this process will appear as written-in Repeatable Run-Out (RRO) for the head positioning servomechanism of HDD. This written-in RRO increases Track Mis-Registration (TMR) that must be compensated. Naturally, the requirements on the accuracy in positioning the write head are more stringent in SSW than in HDD servo system.

(2) The servo sectors of each track must be written perfectly radially coherent with those in the adjacent tracks. Otherwise, some servo data will be degraded or corrupted. In SSW process, this is done by controlling a Phase Lock Loop (PLL) to generate the clock signal and write the timing marks in the servo patterns. The misalignment between the written timing marks and the desired timing marks is measured by timing jitter. Excessive timing jitter causes distortion in the read back signal and 'warping' of the servo sectors.

Therefore, in order to write superior servo patterns, a good SSW servo system is necessary. The remainder of this report is organized as follows. In **section 2**, two control algorithms are developed for SSW position control loop. Iterative Learning Control (ILC) design problems are firstly described and solved by using L_1 optimal control method. In the second approach, SSW position control loop is modeled as a Two-Dimension (2-D) system. A 2-D control scheme is proposed and designed by applying 2-D system theory. **Section 3** designs an adaptive filter using Filtered-X Least Mean Square (FXLMS) algorithm to compensate the timing errors. Finally, **section 4** outlines the conclusions and challenges that need to be tackled.

2 POSITION ERROR COMPENSATION FOR SSW SERVO SYSTEM

In this section, the control issues and motivations in SSW position control loop are stated first. Secondly, a simple ILC structure is proposed for compensating the position errors. The design issue is formulated into L_1 optimization problem. In the third part, SSW position control system is modeled as a 2-D Roesser model (2-D RM). A novel 2-D control algorithm is developed to deal with the issues in the position control loop and to

improve the SSW quality. In both control designs, the conditions for asymptotic convergence and monotonic convergence are presented.

2.1 Control Issues and Objectives in SSW Position Control Loop

A. Radial Error Propagation

During SSW process, each writing step writes a 'memory' of all proceeding track errors. These written-in errors propagate along radial direction, which is the so-called Radial Error Propagation (REP). REP is the main issue in SSW position control loop and SSW process will fail unless REP is controlled no to grow.

The block diagram of SSW position control loop is illustrated in Figure 2.1, which contains a typical track following servo loop with Voice Coil Motor (VCM) $P(z)$ and the feedback compensator $C(z)$.

In this report, the track profile is normalized with respect to the track pitch and is denoted by y. In Figure 2.1, the read head follows the i^{th} track with track profile $y_i(k)$ while the write head write the $(i+1)^{th}$ track with track profile $y_{i+1}(k)$. This is possible because of an offset in the radial direction between the read head and write head.

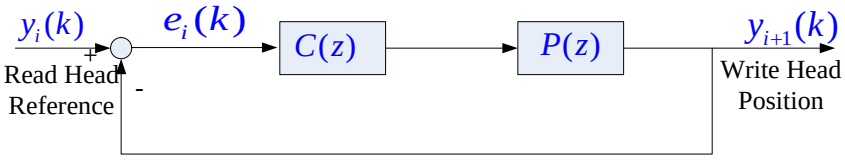

Figure 2.1 Block Diagram of SSW Position Control Loop

It is noted that the transfer function from $y_i(k)$ to $y_{i+1}(k)$ is the complementary sensitivity function:

$$y_{i+1}(k) = T(z)y_i(k) \tag{2.1}$$

where, $T(z) = P(z)C(z)\left(1+P(z)C(z)\right)^{-1}$

Equation (2.1) is the evolution of track profile. In general systems, the gain of $T(z)$, as shown in Figure 2.2, is larger than 1 in some range of frequencies, which amplifies the frequency components of $y_i(k)$ and causes the written-in errors to build up in the radial direction across the disk. So in order to contain the REP, we need

to contain the magnitude of $y_i(k)$. Furthermore, it is desired to design a correction signal to make $\lim_{i\to\infty} y_i = 0$, as illustrated in Figure 2.3.

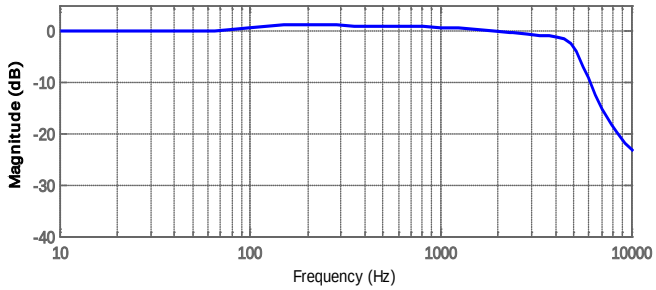

Figure 2.2 Typical Response of Complementary Sensitivity Function

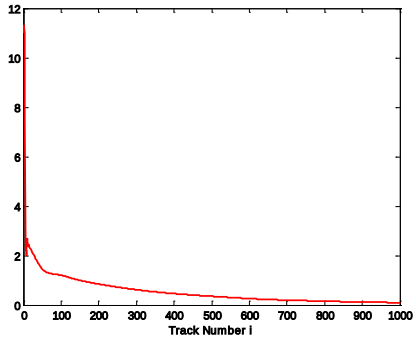

Figure 2.3 Ideal Written Track Profile (i.e., without disturbances)

B. Servo Writing Quality

In addition to containing REP, another significant goal in SSW process is to assure good servowriting quality. An important quantity in this regard is the AC Track Squeeze, which is defined as the minimum spacing between two adjacent tracks as illustrated in Figure 2.4. The definition of AC Track Squeeze is written as,

$$T_{sq}(i) = \min_{k\in[0,N-1]} \{1 + y_{i+1}(k) - y_i(k)\} \times 100\% \tag{2.2}$$

Note that $y_i(k)$ is normalized in tack pitch.

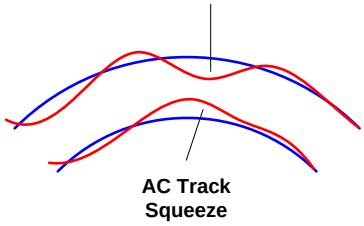

Figure 2.4 Illustration of AC Track Squeeze in HDD

Ideally, it is desired that $T_{sq}(i) < T_{sq}(i+1)$, i.e., $\lim_{i\to\infty} T_{sq}(i) = 100$ (% track pitch), for $i = 0,1,2,\ldots$.

which can be illustrated in Figure 2.5.

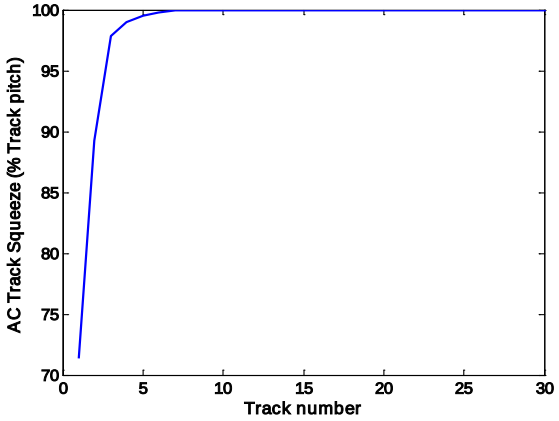

Figure 2.5 Ideal AC Track Squeeze Profile (i.e., without disturbances)

From Equation (2.2), we have,

$$\begin{aligned} T_{sq}(i) &= \left\{1 - \max_{k\in[0,N-1]} \left|y_i(k) - y_{i+1}(k)\right|\right\} \times 100\% \\ &\le \left\{1 - \left(\left\|y_i(\bullet)\right\|_\infty - \left\|y_{i+1}(\bullet)\right\|_\infty\right)\right\} \times 100\% \\ &= \left\{1 + \left\|y_{i+1}(\bullet)\right\|_\infty - \left\|y_i(\bullet)\right\|_\infty\right\} \times 100\% \end{aligned} \tag{2.3}$$

where $\left\|y_i(\bullet)\right\|_\infty$ is defined as the maximum magnitude of the head position signal along one track, i.e., $\left\|y_i(\bullet)\right\|_\infty = \max_{0\le k\le N-1}\left(\left|y_i(k)\right|\right)$, for $i = 0,1\ldots$. It is clearly seen from Equation (2.3) that $T_{sq}(i)$ is related to the maximum magnitude of $y_i(k)$. Therefore we want to control $\left\|y_i(\bullet)\right\|_\infty$ in order to improve the AC Track Squeeze.

2.2 ILC Design for SSW Position Control Loop using L_1 Optimal Control

ILC is loosely based on the paradigm of human learning. In a repetitive process, the information from earlier iterations of the process can be used to improve the performance in the current iteration. The key motivation behind the design of novel ILC scheme is the efficient use of the information from previous iterations so as to maximize the performance, minimize the tracking error, improve robustness and accelerate convergence rate. ILC was originally developed for robots performing repetitive tasks by Arimoto [6] and Uchiyama [7]. ILC

has been implemented in several applications for control of repetitive processes because of its simplicity of design, analysis and implementation.

An ILC based control scheme can be an effective approach to mitigate the REP in SSW position control loop. In this section, a simple ILC scheme is designed. It is followed by the analysis of the conditions for asymptotic convergence and monotonic convergence, which are stronger than that have been discussed by Wu and Tomizuka [1]. Based on these conditions, the ILC design is formulated into L_1 optimal control problem that can be solved by Optimization Programming.

In this section, a correction signal $u_i(k)$ is injected to the position control loop, as shown in Figure 2.6. This configuration is same as the one in Wu and Tomizuka [1].

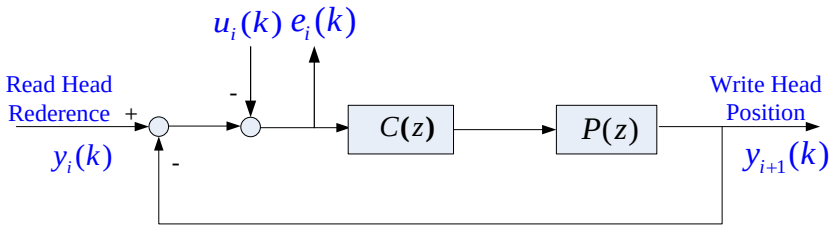

Figure 2.6 Block Diagram of SSW Position Control Loop with ILC

In SSW process, the head position $y_i(k)$ is not measurable, however, the error signal $e_i(k)$ and its previous cycle values $e_{i-1}(k)$ for all $k's$ are available for us to estimate $y_i(k)$. Hence, it is intuitive to use $e_{i-1}(k)$ to generate the correction signal $u_i(k)$,

$$u_i(k) = F(z) \cdot e_{i-1}(k) \tag{2.4}$$

where $F(z)$ is a learning filter to be designed. $F(z)$ has both the causal part and non-causal part, as shown in the following equation:

$$F(z) = \cdots + f_2^N z^2 + f_1^N z + f_0 + f_1^C z^{-1} + f_2^C z^{-2} + \cdots$$

where $f_i^N's$ and $f_i^C's$ are the weighting factors on non-causal and causal error signals respectively.

Since $\{e_{i-1}(k) : 0 \le k \le N-1\}$ is all available from the beginning of the i^{th} iteration, the non-causal part is implementable.

2.2.1 Analysis in Lifted Domain

From Figure 2.6, we have the evolution of track profiles, i.e., the relationship between $y_i(k)$ and $y_{i+1}(k)$:

$$\begin{aligned} y_{i+1}(k) &= T(z)\left[y_i(k) - u_i(k)\right] = T(z)y_i(k) - T(z)F(z)e_{i-1}(k) \\ &= T(z)y_i(k) - T(z)F(z)\left(P(z)C(z)\right)^{-1} y_i(k) \\ &= \left[T(z) - S(z)F(z)\right] y_i(k) \end{aligned} \tag{2.5}$$

where $S(z) = 1/(1 + P(z)C(z))$ is the sensitivity function, and $T(z) = 1 - S(z)$ is the complementary sensitivity function.

By defining the following Super-vectors,

$$y_i = \begin{bmatrix} y_i(0) \\ y_i(1) \\ y_i(2) \\ \vdots \\ y_i(N-1) \end{bmatrix} \quad e_i = \begin{bmatrix} e_i(0) \\ e_i(1) \\ e_i(2) \\ \vdots \\ e_i(N-1) \end{bmatrix} \text{ and } \quad u_i = \begin{bmatrix} u_i(0) \\ u_i(1) \\ u_i(2) \\ \vdots \\ u_i(N-1) \end{bmatrix}$$

where N denotes the total servo sector numbers in one track, the evolution of track profiles in the lifted domain can be derived from Equation (2.5),

$$\begin{aligned} y_{i+1} &= Ty_i - Tu_i = Ty_i - TFe_{i-1} \\ &= Ty_i - TF(PC)^{-1} y_i = \left[T - SF\right] y_i \end{aligned} \tag{2.6}$$

where *S*, *T* and *F* are the markov matrices of $S(z)$ and $T(z)$.

The impulse response of $S(z)$ can be represented as,

$$S(z) = s_0 + s_1 z^{-1} + s_2 z^{-2} + \ldots + s_{N-1} z^{-N+1} + \ldots \tag{2.7}$$

Using its markov parameters s_0, s_1,…, s_{N-1}, we construct *S* as an $N \times N$ matrix:

$$S = \begin{bmatrix} s_0 & 0 & 0 \ldots 0 \\ s_1 & s_0 & 0 \ldots 0 \\ s_2 & s_1 & s_0 \ldots 0 \\ \vdots & \vdots & \vdots \quad \vdots \\ s_{N-1} & s_{N-2} & s_{N-3} \ldots s_0 \end{bmatrix}$$

Matrices *T* and *F* are constructed in the same way.

$$T=\begin{bmatrix} t_0 & 0 & 0\ \dots\ 0 \\ t_1 & t_0 & 0\ \dots\ 0 \\ t_2 & t_1 & t_0\ \dots\ 0 \\ \vdots & \vdots & \vdots \quad \vdots \\ t_{N-1} & t_{N-2} & t_{N-3} \dots t_0 \end{bmatrix} \text{ and } F=\begin{bmatrix} f_0 & f_1^N & f_2^N & \cdots & & \\ f_1^C & f_0 & f_1^N & f_2^N \cdots & & \\ f_2^C & f_1^C & f_0 & f_1^N \cdots & & \\ \vdots & f_2^C & f_1^C & f_0 \cdots & & \\ & \vdots & \vdots & \vdots & f_0 & f_1^N \\ & & & f_2^C & f_1^C & f_0 \end{bmatrix}$$

Note that Equation (2.6) implies that the matrix $\left[T-SF\right]$ is essential in relating the current track and next track profiles.

2.2.2 Asymptotic Convergence Analysis

Definition 2.1: (Asymptotic Convergence for SSW process) SSW process is said to be asymptotically convergent if the head position y_i converges to zero, i.e., $\lim_{i\to\infty} y_i = 0$. It is easy to see that the asymptotic convergence condition for system in Equation (2.6) is,

$$\left|\rho\left(T-SF\right)\right|<1 \tag{2.8}$$

where $\rho\left(T-SF\right)$ denotes the spectral radius of the matrix $\left(T-SF\right)$.

Asymptotic convergence guarantees that the Radial Error Propagation is well contained.

2.2.3 Monotonic Convergence Analysis

To improve the AC Track Squeeze, asymptotic convergence is not enough and there needs a stronger condition.

Definition 2.2: (Monotonic Convergence for SSW process): SSW system is said to be monotonically convergent if the maximum magnitude of written track profile y_i, i.e., $\left\|y_i\right\|_\infty$ decreases successively.

The monotonic convergence can be equivalently expressed as,

$$\left\|y_{i+1}(\bullet)\right\|_\infty < \left\|y_i(\bullet)\right\|_\infty \tag{2.9}$$

For the system in Equation (2.5), it requires

$$\left\| T - SF \right\|_\infty < 1 \tag{2.10}$$

Notice that designing F to satisfy the condition in Equation (2.10) is an L_1 control problem and stronger than condition in Equation (2.8). Under the monotonic convergence condition in Equation (2.9) or (2.10), the peak value of written track profile decreases monotonically, which is followed by the peak of PES also monotonically decreases. As a result, the performance of servowriting (i.e., AC track squeeze) is improved.

Remark: The condition for monotonic convergence in Equation (2.10) is stronger than that has been discussed in [1]: $\left\| y_{i+1}(k) \right\|_2 < \left\| y_i(k) \right\|_2$, which keeps decreasing in the sense of energy. Or equivalently, Equation (2.9) is one sufficient condition of $\left\| y_{i+1}(k) \right\|_2 < \left\| y_i(k) \right\|_2$. Furthermore, $\left\| y_{i+1}(k) \right\|_2 < \left\| y_i(k) \right\|_2$ requires $\left\| T - SF \right\|_2 < 1$, which is an H_∞ control problem.

2.2.4 L_1 Optimal Control Formulation

In this report, the learning filter $F(z)$ is considered as a FIR filter with three causal coefficients and two non-causal coefficients, i.e.,

$$F(z) = f_2^N z^2 + f_1^N z + f_0 + f_1^C z^{-1} + f_2^C z^{-2} \tag{2.11}$$

Now we introduce the following new transfer functions and their markov matrices:

(a) $S_1(z)$ is defined as the one-step advance of $S(z)$, i.e., $S_1(z) = z \cdot S(z)$ and S_1 is its markov matrix. Matrix S_2 is defined as the markov matrix of $S_2(z)$, which is the two-step advance of $S(z)$, i.e., $S_2(z) = z^2 \cdot S(z)$

$$S_1 = \begin{bmatrix} s_1 & s_0 & 0 \ \dots \ 0 \\ s_2 & s_1 & s_0 \ \dots \ 0 \\ s_3 & s_2 & s_1 \ \dots \ 0 \\ \vdots & \vdots & \vdots \quad \vdots \\ 0 & s_{N-1} & s_{N-2} \dots s_1 \end{bmatrix}, \quad S_2 = \begin{bmatrix} s_2 & s_1 & s_0 \ \dots \ 0 \\ s_3 & s_2 & s_1 \ \dots \ 0 \\ s_4 & s_3 & s_2 \ \dots \ 0 \\ \vdots & \vdots & \vdots \quad \vdots \\ 0 & 0 & s_{N-1} \dots s_2 \end{bmatrix} \tag{2.12}$$

(b) Similarly, $S_3(z)$ and $S_4(z)$ are the one-step delay and the two-step delay of $S(z)$, and their corresponding markov matrices are S_3 and S_4.

$$S_3 = \begin{bmatrix} 0 & 0 & 0 \dots 0 \\ s_0 & 0 & 0 \dots 0 \\ s_1 & s_0 & 0 \dots 0 \\ \vdots & \vdots & \vdots \quad \vdots \\ s_{N-2} & s_{N-3} & s_{N-4} \dots 0 \end{bmatrix}, \quad S_4 = \begin{bmatrix} 0 & 0 & 0 \dots 0 \\ 0 & 0 & 0 \dots 0 \\ s_0 & 0 & 0 \dots 0 \\ \vdots & \vdots & \vdots \quad \vdots \\ s_{N-3} & s_{N-4} & s_{N-5} \dots 0 \end{bmatrix} \tag{2.13}$$

Consequently, the matrix SF is expressed as,

$$SF = f_0 \cdot S_0 + f_1^N \cdot S_1 + f_2^N \cdot S_2 + f_1^C \cdot S_3 + f_2^C \cdot S_4 = \sum_{\kappa=0}^{4} S_k f_k \tag{2.14}$$

where $S_0 = S$, $f_1 = f_1^N$, $f_2 = f_2^N$, $f_3 = f_1^C$ and $f_4 = f_2^C$

It is followed by the expression of $\|T - SF\|_\infty$:

$$\|T - SF\|_\infty = \left\| T - \sum_{\kappa=0}^{4} S_k f_k \right\|_\infty = \max_i \left(\sum_{j=1}^{N} \left| T_{ij} - \sum_{\kappa=0}^{4} S_{k\_ij} f_k \right| \right) \tag{2.15}$$

where S_{k_ij} is the (i, j) element of matrix S_k, for $k = 0,1,...,4$.

By introducing Equation (2.15), the condition in Equation (2.10) can be expressed as,

$$\max_i \left(\sum_{j=1}^{N} \left| T_{ij} - \sum_{\kappa=0}^{4} S_{k\_ij} f_k \right| \right) < 1 \tag{2.16}$$

Notice that Inequality (2.16) is an optimization problem.

2.2.5 Consideration of Disturbance and Noise

During the practical HDD SSW process, the disturbances from spindle/disks and the sensor noise always exist. They inevitably deviate the Read/Write heads from the desired track centre and deteriorate the quality of SSW process. Hence, in the simulations, we consider the spindle/disks disturbance and sensor noise, which are shown in the following Figure 2.7. In this block diagram, $d_i(k)$ represents the disk flutter and spindle vibration. The sensor measurement noise is denoted by $n_i(k)$.

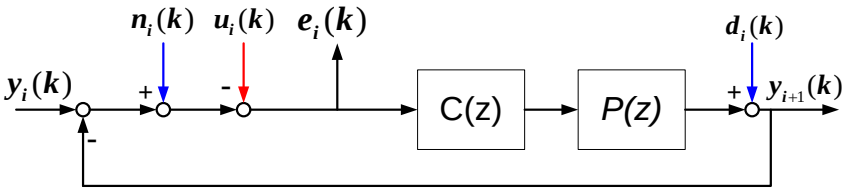

Figure 2.7 SSW Position Control Loop with Disturbance and Noise

By considering $d_i(k)$ and $n_i(k)$, we have a new evolution equation for the track profile,

$$\begin{aligned} y_{i+1} &= Ty_i - Tu_i + Tn_i + Sd_i = Ty_i - TFe_{i-1} + Tn_i + Sd_i \\ &= Ty_i - TF(PC)^{-1}y_i + TF(PC)^{-1}d_{i-1} + Tn_i + Sd_i \\ &= \left[T - SF\right]y_i + Tn_i + Sd_i + SFd_{i-1} \end{aligned} \tag{2.17}$$

From Equation (2.17), it can be seen that the track profile y_{i+1} is affected not only by the current-track disturbance n_i and d_i, but also by the previous-track disturbance d_{i-1}. Since the response from $n_i(k)$ to $y_{i+1}(k)$ is $T(z)$, and that from $d_i(k)$ to $y_{i+1}(k)$ is $S(z)$, the rejection performance on n_i and d_i is decided by $T(z)$ and $S(z)$, which are considered when the feedback compensator $C(z)$ was designed. On the other hand, the rejection performance on d_{i-1} is determined by $S(z)F(z)$. Thus, in order to effectively attenuate d_{i-1}, the filter F(z) should be designed such that $\|SF\|_\infty \le \|S\|_\infty$, or equivalently,

$$\|F\|_\infty \le 1 \tag{2.18}$$

Noting the structure of *F*, i.e.,,

$$F = \begin{bmatrix} f_0 & f_1^N & f_2^N & & \\ f_1^C & f_0 & f_1^N & f_2^N & \\ f_2^C & f_1^C & f_0 & f_1^N & \cdots \\ & f_2^C & f_1^C & f_0 & \cdots \\ & & \vdots & \vdots & f_0 & f_1^N \\ & & & f_2^C & f_1^C & f_0 \end{bmatrix} \tag{2.19}$$

we conclude that $\|F\|_\infty \le 1$ can be rewritten as,

$$\left(\left|f_2^C\right| + \left|f_1^C\right| + \left|f_0\right| + \left|f_1^N\right| + \left|f_2^N\right|\right) \le 1 \tag{2.20}$$

Now the two conditions in equations (2.16) and (2.20) are formulated into one optimization problem to

obtain the feasible values of filter coefficients. This optimization problem can be solved by using Yalmip package [2].

2.2.6 Simulation Results

In this section, the proposed ILC scheme is applied to a benchmark HDD developed by IEEJapan technical committee on Nano-Scale Servo (NSS) system [2006]. The simulated HDD has total servo wedge number of $N = 220$, and the spindle rotation speed is 7200 rpm ; thus the sampling frequency is $220 \times (7200/60) = 26,400$ Hz . The Bode plot of HDD VCM is as shown in Figure 2.8.

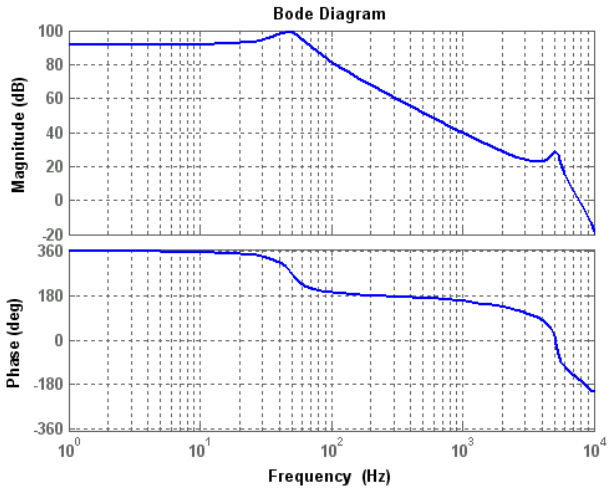

Figure 2.8 Bode Plot of HDD VCM

The performance of learning filter $F(z)$ and $S(z)F(z)$ are firstly examined. Figure 2.9 is the frequency response of the filter $F(z)$. It is clear that its magnitude is below 0 *db* at all frequencies. The comparison of $S(z)$ and $S(z)F(z)$ is shown in Figure 2.10. We learn that $S(z)F(z)$ not only preserves the disturbance attenuation property of $S(z)$ at low frequencies, but also has much lower peak value than $S(z)$; in other words, $S(z)F(z)$ has better rejection performance on d_{i-1} than $S(z)$.

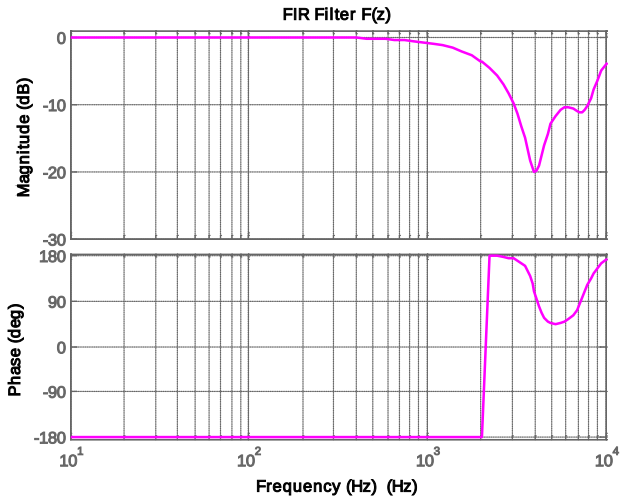

Figure 2.9 Frequency Response of $F(z)$

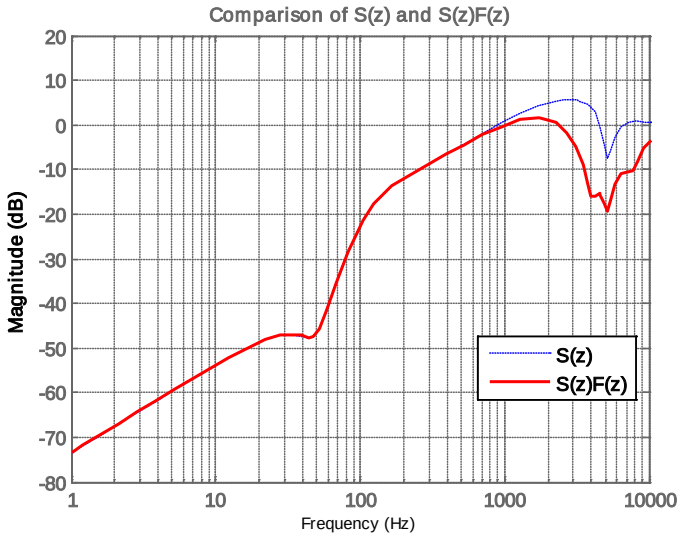

Figure 2.10 Frequency Responses of $S(z)$ *and* $S(z)F(z)$

Figure 2.11 and Figure 2.12 compare the closed-loop responses before and after applying the proposed ILC control law. It is noted that with ILC, the maximum gain of the closed-loop response, i.e., $T(z)-S(z)F(z)$ is less than 1. This condition ensures that the effect of non-circular tracks is diminishing as the track number i increases.

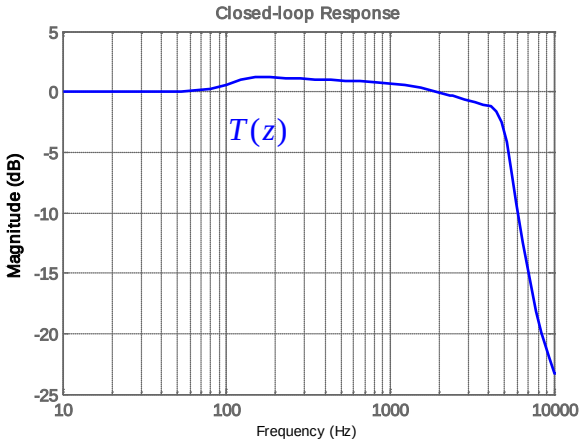

Figure 2.11 Closed-loop Response before applying ILC

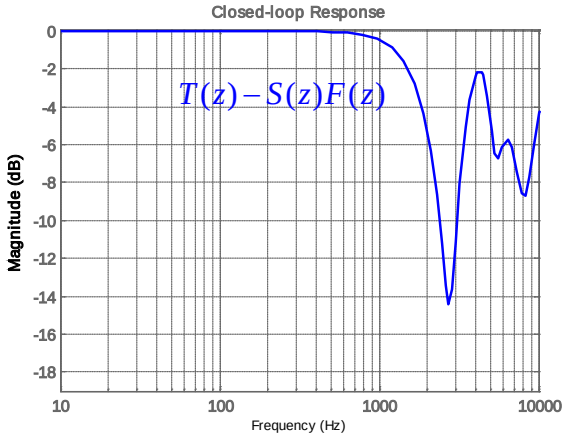

Figure 2.12 Closed-loop Response after applying ILC

The modeled sensor noise is white noise with a sigma value of 1.5% of a track pitch, and that of the disk/spindle disturbance is 1.7% of a track pitch. The first track $y_0(k)$ is assumed to be the seed track and has a sigma value of about 11.0% of a track pitch (See Figure 2.13). In the simulation, total 1000 servo tracks data was collected. Figure 2.14 shows the track profiles with the effect of disturbance and noise. It is observed that the Radial Error Propagation is well contained since the head position y_i converges to some small value. The average one sigma value is about *2.93%* track pitch. This is comparable to the seed track $\boldsymbol{y}_0$.

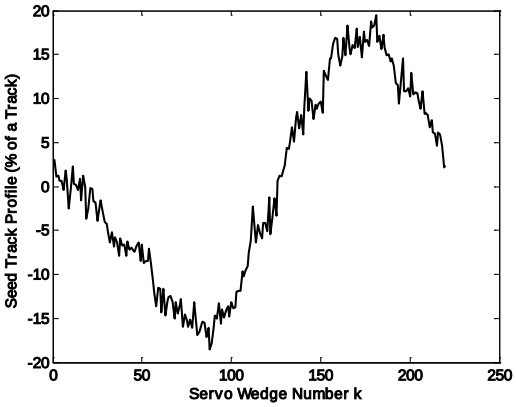

Figure 2.13 Seed Track Profile

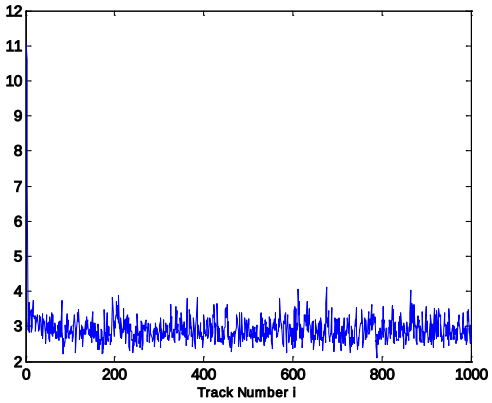

Figure 2.14 Track Profiles of 1000 Tracks

Another important performance measure is the AC track squeeze. The ideal AC track squeeze is one track pitch. When the AC track squeeze value is too small, two adjacent tracks with narrow track spacing may cause some data corruption. The simulation results in Figure 2.15 and Figure 2.16 tell that the average AC track squeeze is about *91.6%* track pitch, which is within the acceptable limit.

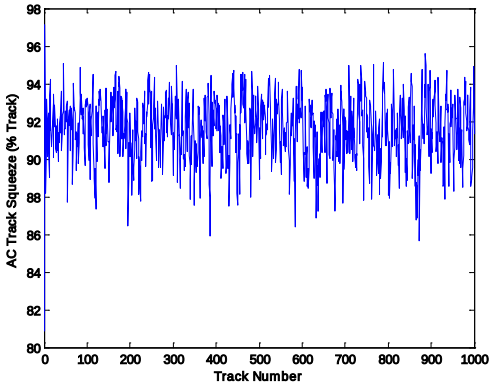

Figure 2.15 AC Track Squeeze

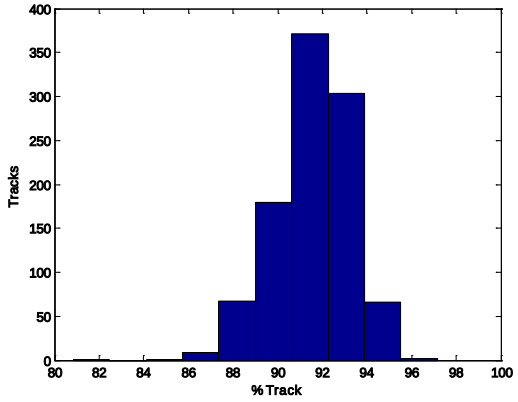

Figure 2.16 Histogram of AC Track Squeeze

2.3 Position Error Compensation using Two-Dimensional (2-D) System Theory

2.3.1 Two-Dimensional (2-D) Control proposal and its advantages

In this section, the dynamics of SSW process is described as Two-Dimensional Roesser Model (2-D RM) [3], [4]. Two-dimensional (2-D) systems are those systems in which the inputs, outputs and states depend on two independent variables. In other words, the dynamics of a 2-D system is propagated along two independent directions. As there are two independent dynamic processes in the 2-D system, we are able to use one of them to reflect the system dynamics in the time domain and the other to reflect the system dynamics in disk rotation domain. In [4], Roesser has developed a well known state-space model for discrete time systems.

There are several motivations and significances of employing 2-D system theory to design and analyze SSW process:

a) SSW process is a 2-D system in nature. The 2-D Roesser Model reveals the 2-D characteristic of SSW process, i.e., its dynamic propagation along the tangential direction and radial direction.

b) Based on the 2-D model, the stability and convergence problems of SSW system can be translated to the stability and convergence problems of 2-D system. And 2-D system theory [3] gives a useful way to show the stability and convergence of the SSW servo system in the time domain and disk rotation domain.

In the following part, the 2-D system theory will be employed to design the feedback controller and feedforward controller together to guarantee the stability and convergence of SSW process along both tangential and radial directions. Effectiveness and feasibility of the proposed control scheme are verified through the computer simulations.

2.3.2 2-D System Theory Review

This subsection will briefly summarize some useful definitions and theories for the 2-D system.

A. State-space Model of 2-D RM Systems

In the 2-D Roesser Model [4], the local state of the system is decomposed into two state components, namely the horizontal state x^h and the vertical state x^v, i.e., $x(k,i)=\begin{bmatrix} x^h(k,i) & x^v(k,i)\end{bmatrix}^T$, where k and i are non-negative integer-valued horizontal and vertical coordinates. $x^h \in \mathbb{R}^{n_1}$ and $x^v \in \mathbb{R}^{n_2}$ are the state components which are propagated horizontally and vertically. Compact matrix form of 2-D Roesser's state-space model is given as,

$$\begin{cases} \begin{bmatrix} x^h(k+1,i) \\ x^v(k,i+1)\end{bmatrix} = \begin{bmatrix} A_{11} & A_{12} \\ A_{21} & A_{22}\end{bmatrix}\begin{bmatrix} x^h(k,i) \\ x^v(k,i)\end{bmatrix} + \begin{bmatrix} B_1 \\ B_2\end{bmatrix} u(k,i) \\ y(k,i)=\begin{bmatrix} C_1 & C_2\end{bmatrix}\begin{bmatrix} x^h(k,i) \\ x^v(k,i)\end{bmatrix} \end{cases} \tag{2.21}$$

Where $u \in \mathbb{R}^r$ is the input vector and $Y \in \mathbb{R}^m$ is the output vector of the 2-D system. The boundary conditions for the system in (2.21) are given by $x^h(0,i)$ and $x^v(k,0)$, $k,i=0,1,2...$.

B. Asymptotic Stability of 2-D RM Systems

A significant issue in 2-D system is the stability. According to [3], the zero-input state trajectory for the system in Equation (2.21), is given by,

$$\begin{bmatrix} x^h(k,i) \\ x^v(k,i)\end{bmatrix} = \sum_{j=0}^{k} A^{k-j,i}\begin{bmatrix} 0 \\ x^v(j,0)\end{bmatrix} + \sum_{l=0}^{i} A^{k,i-l}\begin{bmatrix} x^h(0,l) \\ 0\end{bmatrix} \tag{2.22}$$

where $A^{k,i}$ is the 2-D state transition matrix defined as:

$$A^{k,i} = \begin{cases} I_{n_1+n_2}, & k = i = 0 \\ A^{1,0}A^{k-1,i} + A^{0,1}A^{k,i-1}, & k \geq 0,\ i \geq 0\ \ (k+i \neq 0) \\ 0, & k < 0\ \ or\ \ i < 0 \end{cases} \tag{2.23}$$

and $A^{1,0} = \begin{bmatrix} A_{11} & A_{12} \\ 0 & 0 \end{bmatrix}$ and $A^{0,1} = \begin{bmatrix} 0 & 0 \\ A_{21} & A_{22} \end{bmatrix}$.

The asymptotic stability of 2-D system is defined as follows:

Definition 2.3 [3] The 2-D RM system in Equation (2.21) is said to be asymptotically stable if and only if for zero input $u(k,i) = 0$ and any finite boundary conditions $x^h(0,i)$ and $x^v(k,0)$,

$$\lim_{\substack{k\to\infty\ and/or \\ i\to\infty}} x(k,i) = \lim_{\substack{k\to\infty\ and/or \\ i\to\infty}} \begin{bmatrix} x^h(k,i) \\ x^v(k,i) \end{bmatrix} = 0 \tag{2.24}$$

Theorem 2.1 [3] (1) A_{11} is stable, i.e., $\left|\lambda_i\{A_{11}\}\right| < 1$ for all i; where λ_i's are the eigenvalues of A_{11}; (2) A_{22} is stable; (3) $\begin{bmatrix} A_{11} & A_{12} \\ A_{21} & A_{22} \end{bmatrix}$ is stable; are necessary conditions for the asymptotic stability of 2-D RM system in Equation (2.21).

C. 2-D Z-Transformation [3]

By using the shift operators z_1 and z_2 along the horizontal direction (k) and vertical direction ($\boldsymbol{i}$), 2-D Z-transformation can be defined as:

$$Z\left[y(k,i)\right] = Y(z_1,z_2) = \sum_{k=0}^{\infty}\sum_{i=0}^{\infty} y(k,i) z_1^{-k} z_2^{-i} \tag{2.25}$$

Applying the above Z-transformation to 2-D RM in Equation (2.21) yields the 2-D transfer function matrix,

$$G(z_1,z_2) = \frac{Y(z_1,z_2)}{U(z_1,z_2)} = \begin{bmatrix} C_1 & C_2 \end{bmatrix} \begin{bmatrix} z_1 I - A_{11} & -A_{12} \\ -A_{21} & z_2 I - A_{22} \end{bmatrix}^{-1} \begin{bmatrix} B_1 \\ B_2 \end{bmatrix} \tag{2.26}$$

And the 2-D characteristic polynomial of the system in Equation (2.21) is:

$$d(z_1,z_2) = \det \begin{bmatrix} z_1 I - A_{11} & -A_{12} \\ -A_{21} & z_2 I - A_{22} \end{bmatrix} \tag{2.27}$$

Theorem 2.2 [3]: 2-D Roesser Model system in Equation (2.21) is asymptotically stable if and only if

$$d(z_1, z_2) = \det\begin{bmatrix} z_1 \cdot I_{n_1} - A_{11} & -A_{12} \\ -A_{21} & z_2 \cdot I_{n_2} - A_{22} \end{bmatrix} \neq 0, \quad for \quad |z_1| \geq 1, \quad |z_2| \geq 1 \tag{2.28}$$

By matrix manipulations, Equation (2.28) can be written as,

$$\begin{aligned} & d(z_1, z_2) \\ &= \det(z_1 I_{n_1} - A_{11}) \cdot \det\left(z_2 I_{n_2} - \left[A_{22} + A_{21}(z_1 I_{n_1} - A_{11})^{-1} A_{12}\right]\right) \neq 0, \ \ for\ r\,|z_1| \geq 1, \ |z_2| \geq 1 \\ &= \det(z_2 I_{n_2} - A_{22}) \cdot \det\left(z_1 I_{n_1} - \left[A_{11} + A_{12}(z_2 I_{n_2} - A_{22})^{-1} A_{21}\right]\right) \neq 0, \ \ for\ r|z_1| \geq 1, \ |z_2| \geq 1 \end{aligned} \tag{2.29}$$

From [3], Equation (2.29) is reduced to the following two equivalent conditions:

$$\begin{cases} \det(z_1 I_{n_1} - A_{11}) \neq 0, \ |z_1| \geq 1 \\ \det\left(z_2 I_{n_2} - \left[A_{22} + A_{21}(z_1 I_{n_1} - A_{11})^{-1} A_{12}\right]\right) \neq 0, \ |z_1| = 1, |z_2| \geq 1 \end{cases} \tag{2.30a}$$

$$\begin{cases} \det(z_2 I_{n_2} - A_{22}) \neq 0, \ |z_2| \geq 1 \\ \det\left(z_1 I_{n_1} - \left[A_{11} + A_{12}(z_2 I_{n_2} - A_{22})^{-1} A_{21}\right]\right) \neq 0, |z_2| = 1, |z_1| \geq 1 \end{cases} \tag{2.30b}$$

2.3.3 2-D Representation of SSW Servo System

From Figure 2.1, we can describe the SSW position control loop in the following state-space form:

$$\begin{cases} x_i(k+1) = A_p x_i(k) + B_p u_i(k) \\ y_{i+1}(k) = C_p x_i(k) \end{cases} \tag{2.31}$$

where $(A_p, B_p, C_p, 0)$ is the state space realization of HDD VCM and $u_i(k)$ denotes the control input for VCM.

It can be seen from Equation (2.31) that there exist two independent processes: one reflects the system dynamics along the time domain described by k; the other reflects the dynamics of the disk rotation along the radial direction described by i. From this view point, the 2-D model definitely offers an excellent mathematical model to describe the entire dynamics involved in the SSW position control loop.

In this Section, we reformulate the block diagram of SSW position control loop in Figure 2.1 into the block diagram in Figure 2.17, by defining the 2-D (z_1, z_2) transformation:

$$\begin{cases} y(k+1,i) = z_1 \cdot y(k,i) \\ y(k,i+1) = z_2 \cdot y(k,i) \end{cases} \tag{2.32}$$

i.e., z_1 denotes the delay in time k, and z_2 denotes the delay in iteration i.

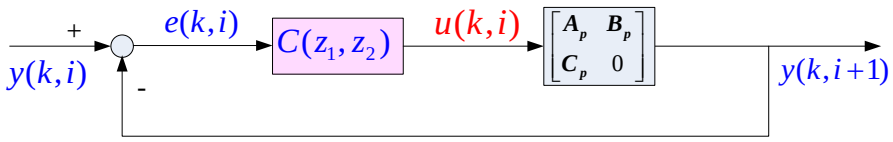

Figure 2.17 Block Diagram of SSW Position Control Loop in 2-D Model

$y(k,i)$ is the Read Head position on the i^{th} track, while $y(k,i+1)$ is the Write Head position on the $(i+1)^{th}$ track. $e(k,i)$ and $u(k,i)$ are the Position Error Signal (PES) and control input respectively. $i = 0,1,2...$ denotes the track number, and $k = 0,1,...,N-1$ denotes the servo wedge number, and N is the total servo wedge number in one track.

Referring to 2-D Roesser Model [4], we define $x(k,i)$ as the horizontal state and $y(k,i)$ as the vertical state. So the 2-D state in SSW system is written as,

$$\begin{cases} x(k,i) = x^h(k,i) \\ y(k,i) = x^v(k,i) \end{cases} \tag{2.33}$$

and Equation (2.31) can be written in 2-D format,

$$\begin{bmatrix} x(k+1,i) \\ y(k,i+1) \end{bmatrix} = \begin{bmatrix} A_p & 0 \\ C_p & 0 \end{bmatrix} \begin{bmatrix} x(k,i) \\ y(k,i) \end{bmatrix} + \begin{bmatrix} B_p \\ 0 \end{bmatrix} u(k,i) \tag{2.34}$$

2.3.4 2-D Controller Design

A. The Proposed Control Law

In Figure 3.1, the PES $e_i(k)$ is expressed as,

$$e(k,i) = y(k,i) - y(k,i+1) = y(k,i) - C_p x(k,i) = [-C_p \quad 1] \begin{bmatrix} x(k,i) \\ y(k,i) \end{bmatrix} \tag{2.35}$$

Note that Equations (2.34) and (2.35) are the 2-D RM of dynamics shown in Figure 3.1, where $u(k,i)$ is the input of 2-D system and $e(k,i)$ is its output.

We know that in the position control loop, only the error signal $e_i(k)$ is measurable. So we need to design an observer to estimate the 2-D state $\begin{bmatrix} x(k,i) \\ y(k,i) \end{bmatrix}$:

$$\begin{cases} \hat{x}(k+1,i) = A_p \hat{x}(k,i) + B_p u(k,i) + L_1 \left(e(k,i) - \hat{e}(k,i) \right) \\ \hat{y}(k,i+1) = C_p \hat{x}(k,i) + L_2 \left(e(k,i) - \hat{e}(k,i) \right) \end{cases} \tag{2.36}$$

where L_1 and L_2 are the observer gains; and the estimated error is written as,

$$\hat{e}(k,i) = \begin{bmatrix} -C_p & 1 \end{bmatrix} \begin{bmatrix} \hat{x}(k,i) \\ \hat{y}(k,i) \end{bmatrix} \tag{2.37}$$

The 2-D control law is designed as,

$$\begin{aligned} u(k,i) &= \begin{bmatrix} -K_1 & -K_2 \end{bmatrix} \begin{bmatrix} \hat{x}(k,i) \\ \hat{y}(k,i) \end{bmatrix} + \sum_{d=1}^{l} F_d \cdot e(k+d, i-1) \\ &= -K_1 \cdot \hat{x}(k,i) - K_2 \cdot \hat{y}(k,i) + F_1 \cdot e(k+1,i-1) + F_2 \cdot e(k+2,i-1) + \ldots F_l \cdot e(k+l,i-1) \\ &= -K_1 \cdot \hat{x}(k,i) - K_2 \cdot \hat{y}(k,i) + F(z_1) \cdot e(k+1,i-1) \end{aligned} \tag{2.38}$$

where $l = 1, 2, \ldots$ is the PES learning steps; K_1 and K_2 are constant matrices and $F(z_1)$ can be regarded as a learning filter to be designed.

With the 2-D control law expressed in Equation (2.38), the system in Figure 2.17 can be equivalently illustrated in Figure 2.18.

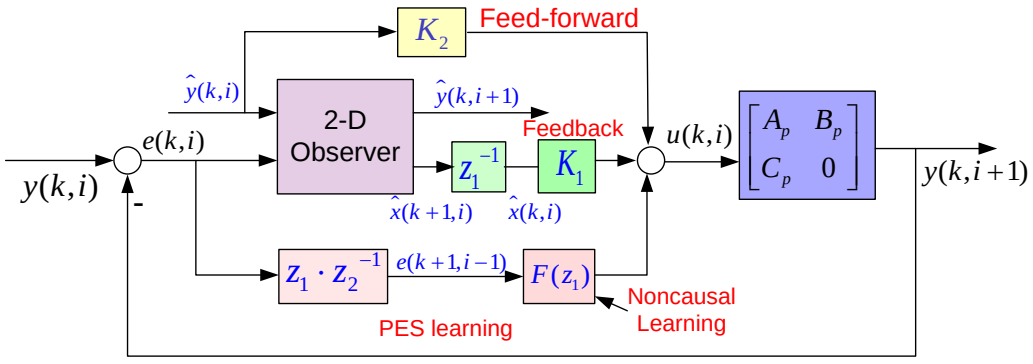

Figure 2.18 Equivalent Block Diagram of Position Control Loop in 2-D Model

***Remarks**:*

(1) K_1 is the feedback gain for the horizontal state $x(k,i)$. (See the feedback loop in Figure 2.18)

(2) K_2 is the feedback gain for the vertical state $y(k,i)$. (See the feedforward loop in Figure 2.18)

(3) The last item in Equation (2.38), i.e., $\sum_{d=1}^{l} F_d \cdot e(k+d, i-1)$, is the *PES* learning from the previous track, and l is the learning step.

B. Design Example

In this subsection, we give one design example of 2-step PES learning. And the control law is expressed as follows.

$$u(k,i) = \begin{bmatrix} -K_1 & -K_2 \end{bmatrix} \begin{bmatrix} \hat{x}(k,i) \\ \hat{y}(k,i) \end{bmatrix} + F_1 \cdot e(k+1, i-1) + F_2 \cdot e(k+2, i-1) \tag{2.39}$$

where F_1 and F_2 are constant matrices to be determined.

By combining and reforming equations (2.34-2.37) and (2.39), we obtain the closed-loop system as,

$$\begin{bmatrix} x(k+1,i+1) \\ \hat{x}(k+1,i+1) \\ y(k+1,i+1) \\ \hat{y}(k+1,i+1) \end{bmatrix} = \begin{bmatrix} A_p & -B_pK_1 & 0 & -B_pK_2 \\ -L_1C_p & (A_p - B_pK_1 + L_1C_p) & L_1 & (-L_1 - B_pK_2) \\ 0 & 0 & 0 & 0 \\ 0 & 0 & 0 & 0 \end{bmatrix} \begin{bmatrix} x(k,i+1) \\ \hat{x}(k,i+1) \\ y(k,i+1) \\ \hat{y}(k,i+1) \end{bmatrix} + \tag{2.40}$$

$$\begin{bmatrix} -B_pF_1C_p & 0 & B_pF_1 & 0 \\ -B_pF_1C_p & 0 & B_pF_1 & 0 \\ C_p & 0 & 0 & 0 \\ -L_2C_p & (C_p + L_2C_p) & L_2 & -L_2 \end{bmatrix} \begin{bmatrix} x(k+1,i) \\ \hat{x}(k+1,i) \\ y(k+1,i) \\ \hat{y}(k+1,i) \end{bmatrix} + \begin{bmatrix} -B_pF_2C_p & 0 & B_pF_2 & 0 \\ -B_pF_2C_p & 0 & B_pF_2 & 0 \\ C_p & 0 & 0 & 0 \\ -L_2C_p & (C_p + L_2C_p) & L_2 & -L_2 \end{bmatrix} \begin{bmatrix} x(k+2,i) \\ \hat{x}(k+2,i) \\ y(k+2,i) \\ \hat{y}(k+2,i) \end{bmatrix}$$

which can be simplified to,

$$\bar{x}(k+1,i+1) = A_1\bar{x}(k,i+1) + A_2\bar{x}(k+1,i) + A_3\bar{x}(k+2,i) \tag{2.41}$$

where $\bar{x}(k,i) = \begin{bmatrix} x(k,i) & \hat{x}(k,i) & y(k,i) & \hat{y}(k,i) \end{bmatrix}^T$ is the state vector;

$$A_1 = \begin{bmatrix} A_p & -B_pK_1 & 0 & -B_pK_2 \\ -L_1C_p & (A_p - B_pK_1 + L_1C_p) & L_1 & (-L_1 - B_pK_2) \\ 0 & 0 & 0 & 0 \\ 0 & 0 & 0 & 0 \end{bmatrix} \quad , \quad A_2 = \begin{bmatrix} -B_pF_1C_p & 0 & B_pF_1 & 0 \\ -B_pF_1C_p & 0 & B_pF_1 & 0 \\ C_p & 0 & 0 & 0 \\ -L_2C_p & (C_p + L_2C_p) & L_2 & -L_2 \end{bmatrix} \quad \text{and}$$

$$A_3 = \begin{bmatrix} -B_pF_2C_p & 0 & B_pF_2 & 0 \\ -B_pF_2C_p & 0 & B_pF_2 & 0 \\ C_p & 0 & 0 & 0 \\ -L_2C_p & (C_p + L_2C_p) & L_2 & -L_2 \end{bmatrix}$$

By defining the new states as,

$$\begin{cases} \phi(k,i) = \bar{x}(k,i+1) - \begin{bmatrix} A_2 & A_3 \end{bmatrix} \begin{bmatrix} \bar{x}(k,i) \\ \underline{x}(k+1,i) \end{bmatrix} \\ \gamma(k,i) = \begin{bmatrix} \bar{x}(k,i) \\ \underline{x}(k+1,i) \end{bmatrix} \end{cases}$$

We can recast Equation (2.41) into,

$$\begin{bmatrix} \phi(k+1,i) \\ \gamma(k,i+1) \end{bmatrix} = \left[\begin{array}{c|cc} A_1 & A_1A_2 & A_1A_3 \\ \hline I & A_2 & A_3 \\ 0 & 0 & 0 \end{array}\right] \begin{bmatrix} \phi(k,i) \\ \gamma(k,i) \end{bmatrix} \tag{2.42}$$

It is noted that Equation (2.42) is 2-D RM, where $\phi(k,i)$ is the horizontal state and $\gamma(k,i)$ is the vertical state.

2.3.5 Stability and Convergence Analysis for Position Control Loop in 2-D

As discussed above, the controlled plant, the proposed control law and the resulting closed-loop system are all represented by a 2-D model. So, in order to design the controller parameters, it is important to analyze the stability and convergence of SSW system in the 2-D model.

A. Asymptotic Convergence Analysis

From Figure 3.1, we know that the *PES* is the difference between the head position on the previous track, i.e., $y(k,i)$ and that on the current track, i.e., $y(k,i+1)$. During SSW, if the control sequence is modified to reduce the PES to be infinitesimal as the track number increases, the SSW position control loop is said to be asymptotically convergent. Mathematically, the following definition is given.

Definition 2.4: SSW position loop is asymptotically convergent if

$$\lim_{i\to\infty} y(k,i) = 0, \quad for \;\; k = 0,1,...,N-1 \tag{2.43}$$

or

$$\lim_{i\to\infty} e(k,i) = 0, \quad for \;\; k = 0,1,...,N-1 \tag{2.44}$$

So Equations (2.43) - (2.44) are equivalent to,

$$\lim_{i\to\infty} \begin{bmatrix} x(k,i) \\ y(k,i) \end{bmatrix} = 0 \text{, for } \; k = 0,1,...,N-1 \tag{2.45}$$

which is apparently the condition for asymptotic stability of SSW position system stated in Equation (2.42).

So we have the following theorem to establish the asymptotic convergence analysis.

Theorem 2.3*:* A sufficient condition for the SSW position system in Equation (2.42) to be asymptotically convergent is that it is asymptotically stable.

Remark**:** The vertical boundary condition $y(k,0)$ is regarded as the seed track profile, which is given prior to SSW process, i.e.,

$$y(k,0) = seed \;\; track \text{, for } k = 0,1,...,N-1$$

and the horizontal boundary value $x(0,i)$ is arbitrarily set to zero during SSW process, i.e.,

$$x(0,i) = 0 \text{, for } i = 0,1,...$$

B. Monotonic Convergence

The AC Track Squeeze defined in Equation (2.2) can be written in 2-D format:

$$T_{sq}(i) = \min_{k\in[0,N-1]} \{1 + y(k,i+1) - y(k,i)\} \times 100\% \;\; \text{(track pitch)} \tag{2.46}$$

And the condition for monotonic convergence is given by:

$$\|y(\bullet, i+1)\|_\infty < \|y(\bullet, i)\|_\infty \tag{2.47}$$

where $\|y(\bullet,i)\|_\infty = \max_{0\le k\le N-1} \left(|y(k,i)|\right), \; i = 0,1....$

Let T denote the transfer function from $y(k,i)$ to $y(k,i+1)$, i.e.,

$$y(k,i+1) = T \cdot y(k,i) \tag{2.48}$$

It is known that the L_1 norm of T is defined as,

$$\|T\|_1 = \frac{\|T \cdot y(k,i)\|_\infty}{\|y(k,i)\|_\infty} \tag{2.49}$$

So the condition in (2.47) is equivalent to,

$$\|T\|_1 < 1 \tag{2.50}$$

Remarks:

(1) It is known that $\|T\|_\infty \le \|T\|_1$, hence $\|T\|_1 < 1$ is stronger than $\|T\|_\infty < 1$ which was analyzed in [1] for ILC design.

(2) let $t(k,i)$ ($k = 0,1,...,N-1; i = 0,1,...$) be the impulse sequence of system T, and the z-transform of this sequence is defined as, $T(z_1, z_2) = \sum_{k=0}^{N-1}\sum_{i=0}^{\infty} t(k,i)\, z_1^{-k} z_2^{-i}$. Thus, the problem of Monotonic Convergence for SSW position control loop can be stated as, $\sum_{k=0}^{N-1}\sum_{i=0}^{\infty}\left|t(k,i)\right| < 1$.

2.3.6 Controller Parameters Design

A. Observer Gains (L_1, L_2) Design

In the first step, the observer gains L_1 and L_2 are designed based on the 2-D state error equation.

Defining the 2-D state error vectors as,

$$\begin{cases} \tilde{x}(k,i) = x(k,i) - \hat{x}(k,i) \\ \tilde{y}(k,i) = y(k,i) - \hat{y}(k,i) \end{cases} \tag{2.51}$$

we obtain the error dynamics as follows,

$$\begin{bmatrix} \tilde{x}(k+1,i) \\ \tilde{y}(k,i+1) \end{bmatrix} = \begin{bmatrix} A_p + L_1 C_p & -L_1 \\ C_p + L_2 C_p & -L_2 \end{bmatrix} \begin{bmatrix} \tilde{x}(k,i) \\ \tilde{y}(k,i) \end{bmatrix} = \begin{bmatrix} A_{e11} & A_{e12} \\ A_{e21} & A_{e22} \end{bmatrix} \begin{bmatrix} \tilde{x}(k,i) \\ \tilde{y}(k,i) \end{bmatrix} \tag{2.52}$$

The above equation is obviously 2-D RM. To design L_1 and L_2, we recall **Theorem 2.1** and **Theorem 2.4** and the following conditions are obtained:

(a) $\rho(A_{e11}) = \rho(A_p + L_1 C_p) < 1$

(b) $\rho(A_{e22}) = \rho(-L_2) < 1$

(c) $\|A_{e11}\| + \|A_{e12}\|(1-\|A_{e22}\|)^{-1}\|A_{e21}\| < 1$

Remarks:

(1) $\rho(A_p + L_1 C_p) < 1$ implies the stability problem of 1-D system $(A_p^{\ T}, -C_p^{\ T})$.

(2) $\rho(-L_2) < 1$ implies $|L_2| < 1$ since L_2 is scalar in this design.

(3) $\|A_{e11}\| + \|A_{e12}\|(1-\|A_{e22}\|)^{-1}\|A_{e21}\| < 1$ derives $|L_2| < \dfrac{1-\|A_p + L_1 C_p\| - \|L_1\| \cdot \|C_p\|}{1-\|A_p + L_1 C_p\| + \|L_1\| \cdot \|C_p\|}$.

B. 2-D State Feedback Gains (K_1, K_2) ***Design***

To design the 2-D state feedback gains K_1 and K_2, we assume that the control law does not contain the PES learning term, i.e.,

$$u(k,i) = \begin{bmatrix} -K_1 & -K_2 \end{bmatrix} \begin{bmatrix} \hat{x}(k,i) \\ \hat{y}(k,i) \end{bmatrix} \tag{2.53}$$

By applying this control signal, we have the closed-loop system as,

$$\begin{bmatrix} x(k+1,i) \\ \hat{x}(k+1,i) \\ y(k,i+1) \\ \hat{y}(k,i+1) \end{bmatrix} = \left[\begin{array}{cc|cc} A_p & -B_p K_1 & 0 & -B_p K_2 \\ -L_1 C_p & (A_p - B_p K_1 + L_1 C_p) & L_1 & (-B_p K_2 - L_1) \\ \hline C_p & 0 & 0 & 0 \\ -L_2 C_p & (C_p + L_2 C_p) & L_2 & -L_2 \end{array}\right] \begin{bmatrix} x(k,i) \\ \hat{x}(k,i) \\ y(k,i) \\ \hat{y}(k,i) \end{bmatrix} = A \begin{bmatrix} x(k,i) \\ \hat{x}(k,i) \\ y(k,i) \\ \hat{y}(k,i) \end{bmatrix} \tag{2.54}$$

By denoting the horizontal state vector as $\bar{x}(k,i) = \begin{bmatrix} x(k,i) \\ \hat{x}(k,i) \end{bmatrix}$, and the vertical state vector as $\bar{y}(k,i) = \begin{bmatrix} y(k,i) \\ \hat{y}(k,i) \end{bmatrix}$, we rewrite equation (2.54) as

$$\begin{bmatrix} \bar{x}(k+1,i) \\ \bar{y}(k,i+1) \end{bmatrix} = \begin{bmatrix} A_{11} & A_{12} \\ A_{21} & A_{22} \end{bmatrix} \begin{bmatrix} \bar{x}(k,i) \\ \bar{y}(k,i) \end{bmatrix} = A \begin{bmatrix} \bar{x}(k,i) \\ \bar{y}(k,i) \end{bmatrix} \tag{2.55}$$

To satisfy **Theorem 2.1** and **Theorem 2.4**, we need the following conditions to design K_1 and K_2.

(a) $\rho(A_{11}) = \rho\begin{bmatrix} A_p & -B_p K_1 \\ -L_1 C_p & A_p - B_p K_1 + L_1 C_p \end{bmatrix} < 1$

(b) $\|A_{11}\|+\|A_{12}\|(1-\|A_{22}\|)^{-1}\|A_{21}\|<1$

Remarks:

(1) $\rho\begin{bmatrix} A_p & -B_pK_1 \\ -L_1C_p & A_p-B_pK_1+L_1C_p \end{bmatrix}<1$ implies the stability problem of 1-D systems (A_p, B_p) and $(A_p{}^T, -C_p{}^T)$ since $\begin{bmatrix} A_p & -B_pK_1 \\ -L_1C_p & A_p-B_pK_1+L_1C_p \end{bmatrix}$ satisfies the Separation Principle.

(2) $\|A_{11}\|+\|A_{12}\|(1-\|A_{22}\|)^{-1}\|A_{21}\|<1$ can derive:

$$\left\|\begin{bmatrix} 0 & -B_pK_2 \\ L_1 & -B_pK_2-L_1 \end{bmatrix}\right\| < \frac{1-\left\|\begin{bmatrix} A_p & -B_pK_1 \\ -L_1C_p & A_p-B_pK_1+L_1C_p \end{bmatrix}\right\|}{\left(1-\begin{bmatrix} 0 & 0 \\ L_2 & -L_2 \end{bmatrix}\right)^{-1}\cdot\left\|\begin{bmatrix} C_p & 0 \\ -L_2C_p & C_p+L_2C_p \end{bmatrix}\right\|}$$

which can be used to calculate K_2.

C. PES Learning Gains (F_1, F_2) ***Design***

By employing **Theorem 2.1** and **Theorem 2.4** again, the following conditions are derived to guarantee the asymptotic stability and convergence of SSW system in Equation (2.42).

(a) $\rho(A_1)<1$

(b) $\rho(A_2)<1$

(c) $\|A_1\|+\|A_1A_2 \;\; A_1A_3\|\left(I-\left\|\begin{bmatrix} A_2 & A_3 \\ 0 & 0 \end{bmatrix}\right\|\right)^{-1}<1$

Remarks:

(1) $\rho(A_1)<1$ implies $\rho\left(\begin{bmatrix} A_p & -B_pK_1 \\ -L_1C_p & (A_p-B_pK_1+L_1C_p) \end{bmatrix}\right)<1$ which has been satisfied when designing K_1.

(2) $\rho(A_2)<1$ implies $|L_2|<1$ and $F_1<\frac{1}{\rho(B_pC_p)}$.

(3) $\|A_1\|+\|A_1A_2\|\left(I-\|A_2\|\right)^{-1}<1$ derives matrix F_2.

2.3.7 Simulations

Same as in Section 2.2.5, we consider the disturbance and sensor noise in the simulations, as shown in Figure 2.19.

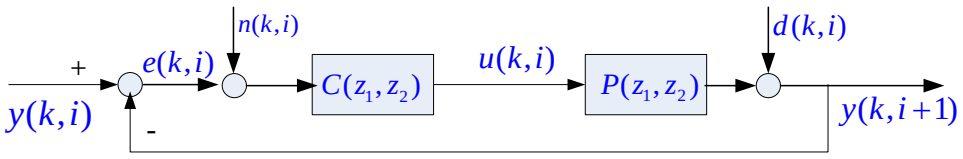

Figure 2.19 Block Diagram of SSW Servo System with Disturbance and Sensor Noise

In the figure, $n(k,i)$ denotes the sensor noise due to PES demodulation and $d(k,i)$ is the disk/spindle disturbance.

The HDD model used for simulations is same as that in Section 2.2.6.

Summarized below are the simulation results using 2-step PES learning control scheme in Equation (2.39). The controller parameters $(K_1, K_2, L_1, L_2, F_1, F_2)$ are listed in the following Table 1.

Table 1 Controller Parameters $(K_1, K_2, L_1, L_2, F_1, F_2)$

K_1	K_2	L_1	L_2	F_1	F_2
[-.9637 1.8102 -.0639 -.238]	**-.0586**	**[.0007 -.0009 .0068 .0245]**	**.011**	**-.0018**	**-.01**

The seed track $y(k,0)$ is same as what used in ILC design, which is plotted in Figure 2.12. In the simulations, total 1000 tracks are propagated.

One sigma values (i.e., standard deviation) of the first one thousand self servo-written tracks are depicted in Figure 2.20. It is apparent that the written tracks converge to a steady value range and its average sigma value is about 1.71% of a track pitch, which is much smaller than that of seed track and within the acceptable limit.

Figure 2.21 plots the AC track squeeze (T_{sq}) and its distribution is depicted in Figure 2.22. The mean AC track squeeze is 93.40% of a track pitch, which shows good quality of servowriting.

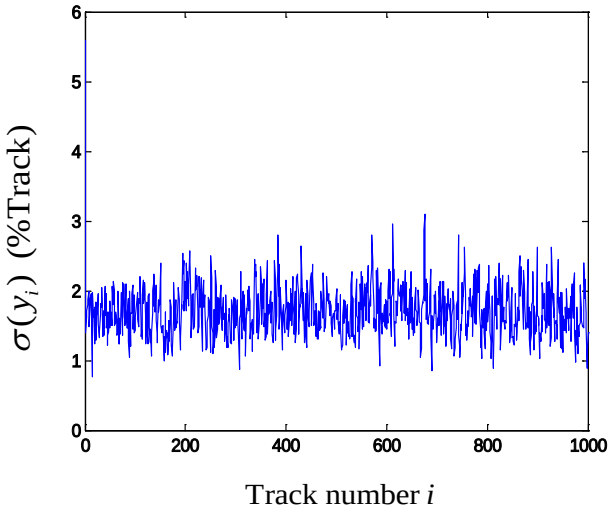

Figure 2.20 Sigma Value of 1000 SSW Written Tracks (% Track)

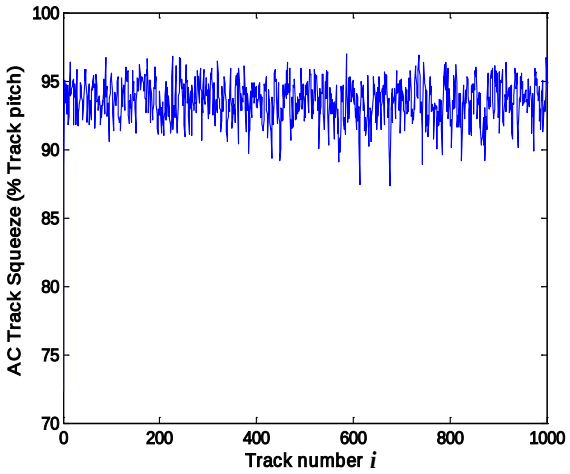

Figure 2.21 AC Track Squeeze (% Track)

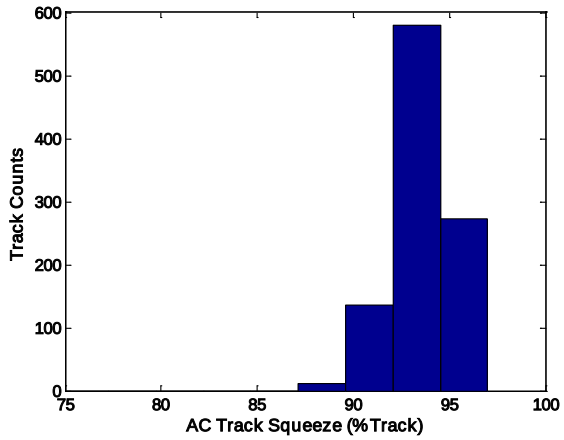

Figure 2.22 Histogram of AC Track Squeeze

Figure 2.23 shows one sigma value of *PES* and its mean is 3.19% track pitch. It also proves good performance of the proposed 2-D control scheme.

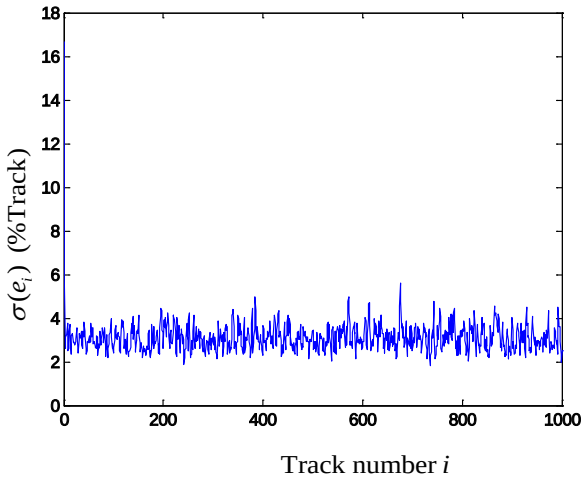

Figure 2.23 Sigma Value of PES (% Track)

3 TIMING ERROR COMPENSATION FOR SSW SERVO SYSTEM

In this section, a control scheme based on Adaptive Feedforward Compensation (AFC) is proposed for SSW timing control loop. An adaptive filter is designed to minimize the closure error in one track and contain the timing error propagation from track to track. The Filtered-X Least Mean Square (FXLMS) technique is used for designing the adaptive filter.

3.1 Timing System in SSW

In SSW process, in order to ensure proper alignment of the servo sectors, the propagation of servo patterns has to be synchronized to the seed clock track or the reference timing marks in previous track. Generally, the seed clock track is prewritten at the Outer Diameter (OD) of a disk by a separated clock head before the SSW process. To write a stable and accurate clock signal in presence of the media defects and disk/spindle disturbances, a Phase Lock Loop (PLL) is generally employed, as shown in Figure 3.1.

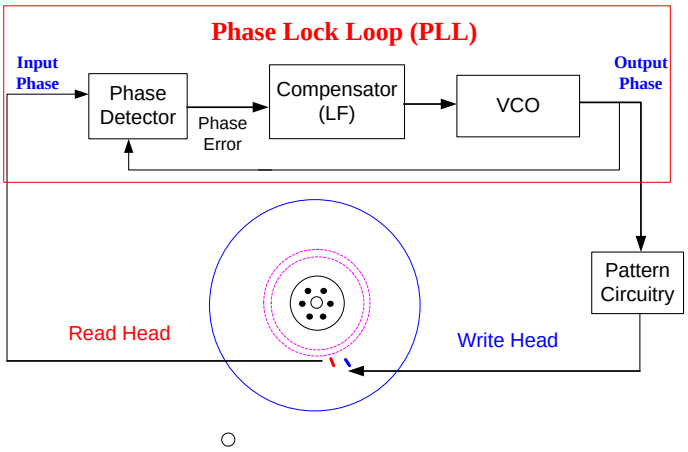

Figure 3.1 PLL in SSW Process

The PLL in Figure 3.1 comprises a Voltage Controlled Oscillator (VCO) for generating a write clock signal used to propagate the servo sectors across the disk during SSW process. The difference between the reference phase signal and output phase signal goes though the Phase Detector (PD) and generates the phase error. The phase error is filtered by the Loop Filter (LF) to generate the VCO control signal.

The block diagram of linearized PLL is shown in Figure 3.2. where input $\phi_i(k)$ denotes the head phase signal in current track and output $\phi_{i+1}(k)$ denotes the head phase signal in the next track. $e_i(k)$ is the phase error generated by the PD; k_p is the gain of PD and $C(z)$ denotes the transfer function of LF which is generally a low-pass filter. The VCO is normally modeled as an integrator. The phase signal is defined in the next section.

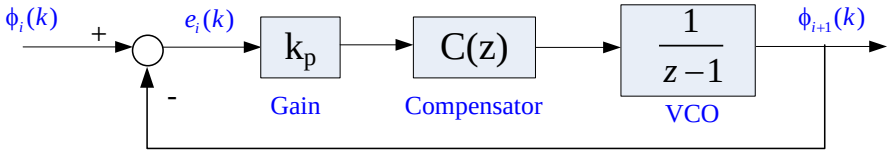

Figure 3.2 Block Diagram of Linearized PLL in SSW Timing Control Loop

3.2 Control Problems in SSW Timing Control Loop

3.2.1 Phase Definition

Let us assume that there are N timing marks in one track (see the solid lines in Figure 3.3). Ideally, they are evenly spaced and marked by $t(0)$, $t(1),\ldots,t(N-1)$. But in practice, these timing marks are not even due to the written-in timing jitters. In Figure 3.3, the dashed lines marked by $t'(0)$, $t'(1),\ldots,t'(N-1)$ are used to denote the actual timing marks.

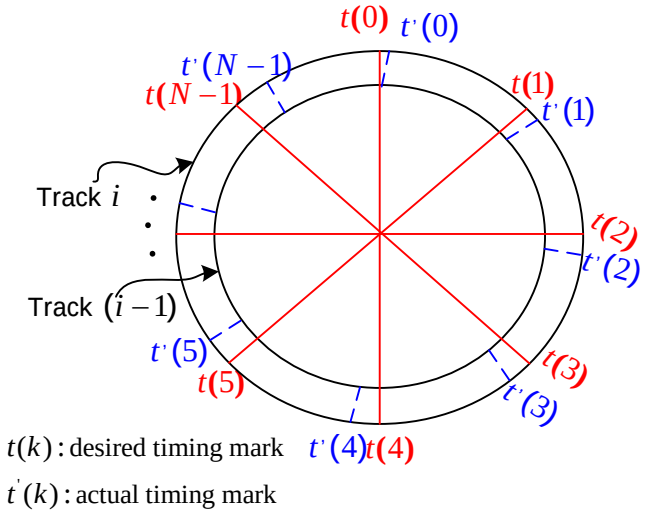

Figure 3.3 Illustration of Timing Marks in Servo Patterns

Definition 3.1: The difference between the desired timing mark and the actual timing mark is called Timing Jitter corresponding to the k^{th} timing mark, i.e.,

$$\Delta t(k) = t'(k) - t(k) \tag{3.1}$$

Definition 3.2: The phase corresponding to the k^{th} timing mark is given by the following equation,

$$\phi(k) = \frac{\left(t'(k) - t(k)\right) \cdot 2\pi \,/\, N}{T_s \,/\, N} = \frac{\Delta t(k) \cdot 2\pi}{T_s} \tag{3.2}$$

where T_s denotes the spindle revolution period.

Note that the phase is a normalized timing jitter.

3.2.2 Problem Statements in Timing Control Loop

During SSW process, $t(k)$ and $t'(k)$ are expected to be same; in other words, the timing jitters are unwanted. Therefore, in order to eliminate the timing jitters, an effective control scheme is necessary to resolve the control issues in SSW timing control loop. There are two main issues in this control loop.

(1) The first important issue is the closure error in one track, which is the phase propagation along circumferential direction. As shown in Figure 3.4, d_k is used to denote the angular distance between two adjacent timing marks $t'(k-1)$ and $t'(k)$, wherein the angular difference between $t'(0)$ and $t'(N-1)$ is named timing closure d_N, i.e., $d_N = 2\pi - \sum_{k=1}^{N-1} d_k$. The difference between d_N and the ideal angular distance in two adjacent servo sectors is defined as the closure error Δd, which is written as $\Delta d = d_N - 2\pi/N$. Closure error Δd is unwanted because it adversely disturbs PLL operation and affects the servo propagation process.

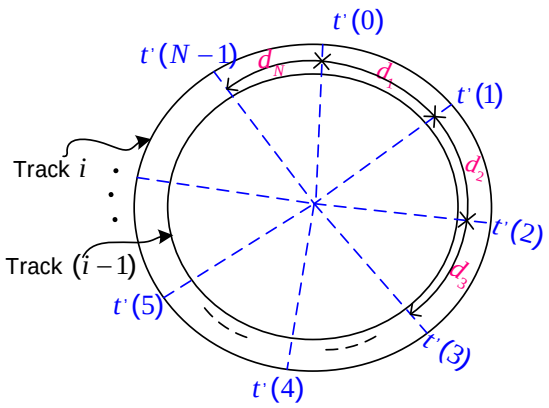

Figure 3.4 Illustration of Angular Distance between Adjacent Sectors

(2) The other significant issue in the timing control loop is the track-to-track timing error propagation, i.e., the phase propagation along radial direction. When the PLL is synchronized to propagate the servo sectors, some disk disturbance, spindle disturbance and sensor noise are amplified by the loop. These components of timing jitters will propagate from track to track and grow unboundedly, resulting in ‘wandering’ or ‘warping’ of servo sectors across the disk surface, as illustrated in Figure 3.5. The ‘warping’ of servo sectors deteriorates the quality of the product servo patterns.

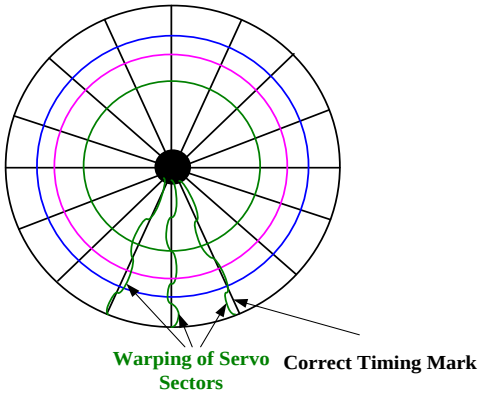

Figure 3.5 Warping of Servo Sectors on the Disk

Hence, in order to resolve the above two issues and improve SSW quality, there is a need to minimize the closure error in one track and attenuate the timing error propagation from track to track.

3.3 Adaptive Filter Design for Timing Control Loop

3.3.1 Modeling of Timing Control Loop

The block diagram for timing control loop is shown in Figure 3.6, which is a simplified form of Figure 3.2. In the figure, $P(z)$ is the PLL open loop transfer function, i.e., $P(z)=\dfrac{k_p \cdot C(z)}{z-1}$.

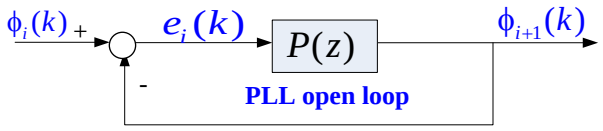

Figure 3.6 Block Diagram for Timing Control Loop

It is noticed that the closed-loop in Figure 3.6 can be equivalently represented in the open loop form in Figure 3.7, where $S(z)$ is the sensitivity function, i.e.,

$$S(z)=\frac{1}{1+P(z)} \tag{3.3}$$

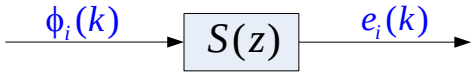

Figure 3.7 Open Loop Representation of Figure 3.6

Definition 3.3: $e_i(k)$ in Figure 3.6 and Figure 3.7 is the timing error between two adjacent tracks for the same sector, i.e.,

$$e_i(k) = \phi_i(k) - \phi_{i+1}(k) \tag{3.4}$$

It is called *the Radial Timing Error*.

Definition 3.4*:* The timing error between two adjacent sectors in the same track is defined as:

$$\varepsilon_i(k) = \phi_i(k) - \phi_i(k-1) \tag{3.5}$$

It is called *the Circumferential Timing Error*.

3.3.2 Adaptive Filter Design for Timing Control Loop

In this section, an Adaptive Feedforward Compensation (AFC) scheme based on Filtered-X Least Mean Square (FXLMS) algorithm will be proposed.

A. Adaptive Feedforward Compensation (AFC)

The general structure of AFC is shown in Figure 3.8. The AFC aims to generate the input of a dynamic system $S(z)$ so that its output follows the desired output $x_i(k)$. The scheme consists of two main elements: an adaptive filter $W(z)$ and an LMS algorithm block. The LMS algorithm adjusts the coefficients of $W(z)$ to minimize the performance index. In Figure 3.8, the reference signal $r_i(k)$ is filtered by $S(z)$ before it is utilized by the LMS algorithm to adjust the filter coefficients. Because of this filtering notion, the adaptive LMS algorithm is called the Filtered-X LMS algorithm.

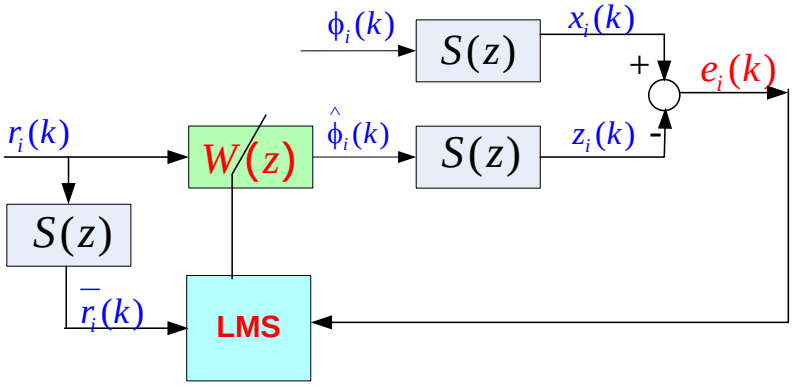

Figure 3.8 Block Diagram of AFC using FXLMS Algorithm

B. The Proposed Control Scheme

It is known that the radial timing error $e_i(k)$ in Figure 3.6 and Figure 3.7 is the only measurable signal in the timing system, that is to say, the head phase signal $\phi_i(k)$ is not measurable for designing the filter. So it is desired to estimate $\phi_i(k)$ and approximate the circumferential timing error $\varepsilon_i(k)$ which will be used as well as the radial timing error $e_i(k)$ to contain the closure error and attenuate the timing error propagation. Note that the estimated head signal $\hat{\phi}_i(k)$ in Figure 3.8 serves as a feed-forward control signal to be designed, as shown in Figure 3.9. We note that the closer to $\phi_i(k)$ $\hat{\phi}_i(k)$, the smaller the radial timing error $e_i(k)$. At the same time, the closure error in one track will also be contained if the radial timing error $e_i(k)$ and circumferential timing error $\varepsilon_i(k)$ are both considered in the design of the adaptive filter in FXLMS. This will be discussed in the following discussion.

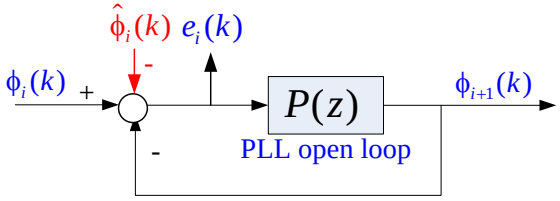

Figure 3.9 Timing Control Loop with the Feedforward Correction Signal $\hat{\phi}_i(k)$

The proposed control scheme is illustrated in Figure 3.10, where $W(z)$ is an adaptive filter to be designed for obtaining the estimated head phase signal $\hat{\phi}_i(k)$. A popular choice of $W(z)$ is a Finite Impulse Response (FIR) digital filter. Notice that FIR filters are always stable. The class of FIR adaptive filters using FXLMS algorithm is well known regarding its convergence conditions and steady state performance. Assume the FIR filter $W(z)$ has the same length as the number of servo sectors in one track:

$$W(z) = w_i(0) + w_i(1)z^{-1} + w_i(2)z^{-2} + \ldots + w_i(N-1)z^{-N+1} \tag{3.6}$$

Remark: $w_i(k)$ in Equation (3.6) denotes the filter coefficient for the k^{th} servo sector in the i^{th} track.

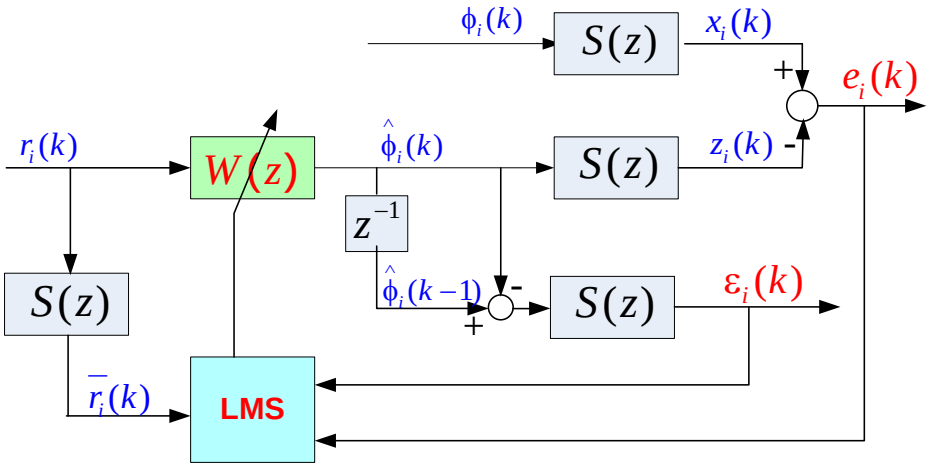

Figure 3.10 The Proposed Control Scheme for Timing Control Loop

The adaptive filter $W(z)$ receives the reference input $r_i(k)$ and generates the estimated head signal $\hat{\phi}_i(k)$ so that the system output $e_i(k)$ is ideally zero. To simplify the design, the reference signal $r_i(k)$ is chosen as an impulse train, i.e.,

$$r_i(k) = \begin{cases} 1 & k = 0,\ i = 1,2,\ldots \\ 0 & \text{otherwise} \end{cases} \tag{3.7}$$

The sensitivity function $S(z)$ in Equation (3.3) is generally given by its markov coefficients, $s(k)$, $k = 0,1,\ldots$, as shown in the following equation.

$$S(z) = s(0) + s(1)z^{-1} + s(2)z^{-2} + \ldots + s(N-1)z^{-N+1} + \ldots \tag{3.8}$$

Furthermore, because the length of $W(z)$ is selected as N, its k^{th} coefficient is equal to the estimated head signal $\hat{\phi}_i(k)$ i.e.,

$$\hat{\phi}_i(k) = w_i(k) \quad \text{for } k = 0,1,\ldots,N\text{-}1;\ i = 1,2,\ldots \tag{3.9}$$

Similarly, the filtered reference signal $\bar{r}_i(k)$ can be written as,

$$\bar{r}_i(k) = s_i(k) \text{ for } k = 0,1,\ldots,N\text{-}1;\ i = 1,2,\ldots \tag{3.10}$$

Notice that by introducing the feed-forward signal $\hat{\phi}_i(k)$, the timing errors $e_i(k)$ and $\varepsilon_i(k)$ in equations (3.4) and (3.5) are rewritten as:

$$\begin{aligned} e_i(k) &= x_i(k) - z_i(k) = x_i(k) - \sum_{j=0}^{\infty} s(j) \cdot \hat{\phi}_i(k-j) \\ &= x_i(k) - \sum_{j=0}^{\infty} s(j)\left[w_i(k-j)\right] \end{aligned} \tag{3.11}$$

$$\begin{aligned} \varepsilon_i(k) &= S(z)\left(\hat{\phi}_i(k\text{-}1) - \hat{\phi}_i(k)\right) = \sum_{j=0}^{\infty} s(j)\left(\hat{\phi}_i(k\text{-}1-j) - \hat{\phi}_i(k-j)\right) \\ &= \sum_{j=0}^{\infty} s(j)\left[w_i(k-1-j) - w_i(k-j)\right] \end{aligned} \tag{3.12}$$

where we have noted Equation (3.9).

C. Design Analysis

This subsection describes the procedure of designing the adaptive filter $W(z)$ to estimate the head signal $\hat{\phi}_i(k)$ and circumferential timing error $\varepsilon_i(k)$. Two definitions are firstly introduced.

Definition 3.5: The circumferential timing error energy for one sector is defined as:

$$\beta_i(k) = \varepsilon_i^2(k) = \left(\sum_{j=0}^{\infty} s(j)\left[w_i(k-1-j) - w_i(k-j)\right] \right)^2 \tag{3.13}$$

Definition 3.6: The total radial timing error energy for one track is defined as:

$$\alpha_i = \sum_{k=0}^{N-1} e_i^2(k) = \sum_{k=0}^{N-1} \left(x_i(k) - \sum_{j=0}^{\infty} s(j)\left[w_i(k-j)\right] \right)^2 \tag{3.14}$$

FXLMS algorithm is a method that ensures the energies $\beta_i(k) = \varepsilon_i^2(k)$ and $\alpha_i = \sum_{k=0}^{N-1} e_i^2(k)$ to be minimum by adjusting the filter coefficients $w_i(k)$ adaptively. Therefore, the design problem is equivalent to two minimization problems.

(1) Minimize the circumferential timing error energy for one sector $\beta_i(k) = \varepsilon_i^2(k)$:

It is considered that the filter coefficient $w_i(k)$ is repeatedly corrected in order to minimize the square error $\beta_i(k) = \varepsilon_i^2(k)$. The adjustment of $w_i(k)$ is based on the gradient of $\beta_i(k)$ with respect to $w_i(k)$. For this purpose, we differentiate $\beta_i(k)$ with respect to the filter coefficient $w_i(k)$. Noting Equation (3.13), the following equation is obtained.

$$\frac{\partial \beta_i(k)}{\partial w_i(k)} = 2\varepsilon_i(k)\left(-s(0)\right) = -2\varepsilon_i(k)\cdot \bar{r}_i(0) \tag{3.15}$$

where we have noted Equation (3.10).

By using LMS algorithm, the update equation for $w_i(k)$ at the k^{th} sector is expressed as,

$$w_i^{l+1}(k) = w_i^l(k) + \mu_1 \varepsilon_i^l(k)\bar{r}_i(0) \tag{3.16}$$

where μ_1 is the step size parameter; $l = 1, 2, \ldots, L$ denotes the l^{th} iteration for updating the filter coefficient $w_i(k)$ and L is the number of iterations to be decided by the designer. Equation (3.16) means that the filter coefficients $w_i(k)$ is updated in one track (i.e., for $k = 0,1,...,N-1$) L times before going to next track.

(2) Minimize the total radial timing error energy along one track $\alpha_i = \sum_{k=0}^{N-1} e_i^2(k)$:

In this minimization problem, the filter coefficient vector $w_i = \left[w_i(0) \;\; w_i(1) \;\; \cdots \;\; w_i(N-1)\right]^T$ (i.e., the filter coefficients in one track) is updated for next track minimize the error energy $\alpha_i = \sum_{k=0}^{N-1} e_i^2(k)$. By differentiating both sides in Equation (3.14) partially with respect to $w_i(n)$ ($n = 0,1,...,N-1$), we have the following equation.

$$\begin{aligned} \frac{\partial \alpha_i(k)}{\partial w_i(n)} &= \sum_{k=0}^{N-1} 2\left\{x_i(k) - \sum_{j=0}^{\infty} s(j)\left(w_i(k-j)\right)\right\}\left\{-\sum_{j=0}^{\infty} s(k-n)\right\} \\ &= -\sum_{k=0}^{N-1} 2e_i(k)\bar{r}_i(k-n) \end{aligned} \tag{3.17}$$

where we have noted Equation (3.10).

By using LMS algorithm, the update equation for $w_i(k)$ is expressed as,

$$w_{i+1}(k) = w_i(k) + \mu_2 \left(\sum_{n=0}^{N-1} e_i(k)\bar{r}_i(k-n) \right) \tag{3.18}$$

where μ_2 is the step size parameter. After $w_{i+1}(k)'s$ are obtained, the head starts to write the timing marks on the $(i+1)^{th}$ track. Then, the sectors in the $(i+1)^{th}$ track iteratively update $w_{i+1}^l(k)$ L times by using the update algorithm in Equation (3.16), and so on.

Remark: Minimization of $\beta_i(k) = \varepsilon_i^2(k)$ is equivalent to minimizing the closure error in one track; and minimization of $\alpha_i = \sum_{k=0}^{N-1} e_i^2(k)$ is to attenuate the timing error propagation.

By combining equations (3.16) and (3.18), the AFC with FXLMS algorithm for updating the filter coefficients on the whole disk surfaceis described by the following equations:

$$\begin{cases} \bar{w}_i^{l+1}(k) = \bar{w}_i^{l}(k) + \mu_1 \varepsilon_i^{l}(k)\bar{r}_i(0) \\ \text{with I.C.:} \quad \bar{w}_i^{1}(k) = w_i(k) \end{cases} \tag{3.19a}$$

$$w_{i+1}(k) = \bar{w}_i^{L}(k) + \mu_2 \left(\sum_{n=0}^{N-1} e_i^{L}(k)\bar{r}_i(k-n) \right) \tag{3.19b}$$

for $l = 1, 2, \ldots, L; \quad k = 0, 1, \ldots, N-1; \; i = 1, 2, \ldots.$

Remark: Using the above equations, we have the filter coefficient $w_i(k)$ for each servo sector which is an optimal value to ensure minimum closure error and minimum timing error propagation.

3.4 Simulation Results

In the numerical simulation study, the mechanical jitter $d_i(k)$ and the noise jitter $n_i(k)$ are taken into consideration, as shown in Figure 3.11.

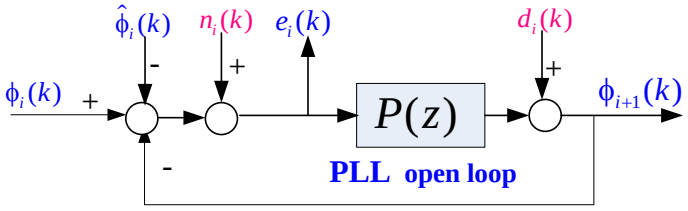

Figure 3.11 Timing Control Loop with Jitters

Figure 3.12 shows the frequency response of PLL open loop $P(z)$ used in the simulations.

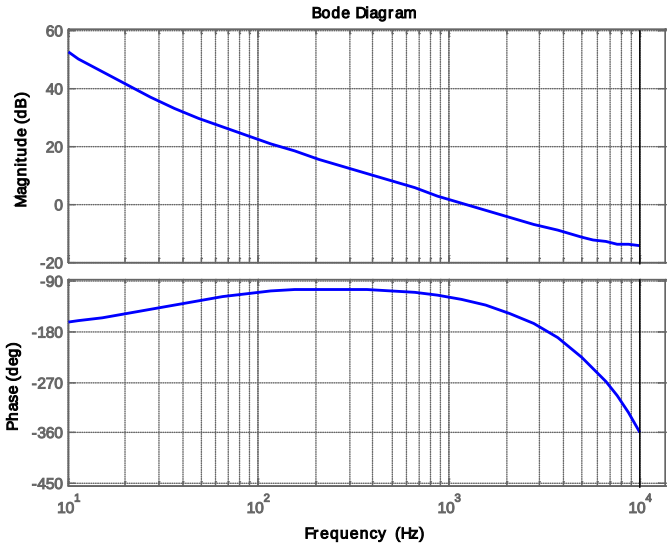

Figure 3.12 Frequency Response of PLL Open Loop $P(z)$

Figure 3.13 compares the frequency responses of the adaptive filter $W(z)$ in the 1st, the 20th and the 800th tracks. To show the feasibility of the proposed control method, the ILC structure presented in section 2.2 was also designed for the timing control loop and its results are compared with the AFC method. Figure 3.14 shows the comparison of the profile of $\hat{\phi}_i(k)$ in the 1000th track. We can see that with the proposed control scheme, the write head reached a much smaller phase than the phase attained by the ILC method and the phase of the seed track (i.e., $i = 0$). The timing jitter in the proposed control scheme is $0.003T_s$ while that in ILC scheme is $1.277T_s$. Both of them are comparable to that in the seed track ($1.512T_s$).

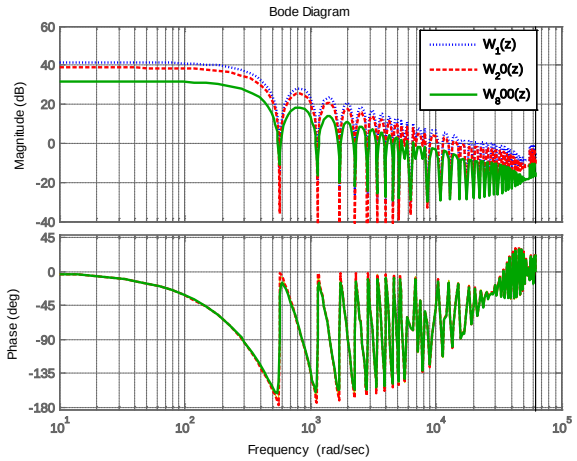

Figure 3.13 Frequency Responses of Adaptive Filter $W(z)$ in Different Tracks

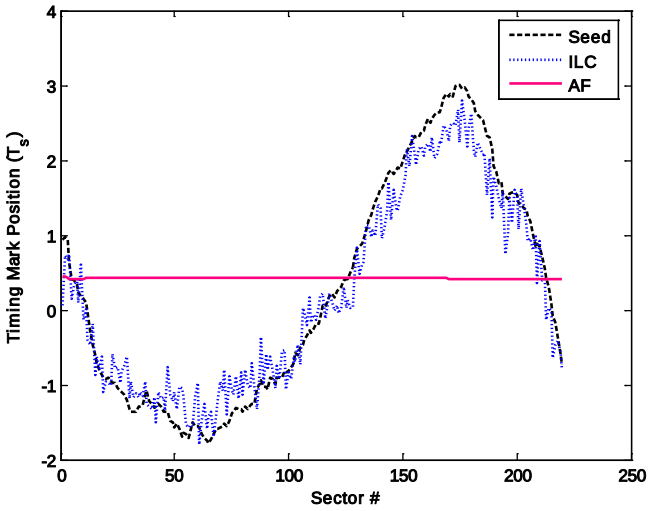

Figure 3.14 Comparison of Phase Profile $\hat{\phi}_i(k)$

The profiles of circumferential timing error ε and radial timing error e are compared in Figure 3.15 and Figure 3.16. Again, it is apparent that the proposed control approach attains a smaller circumferential timing error ($0.031T_s$) and a smoother radial timing error ($0.282T_s$) which compare to ILC results of $0.25T_s$ circumferential timing error and $0.298T_s$ radial timing error.

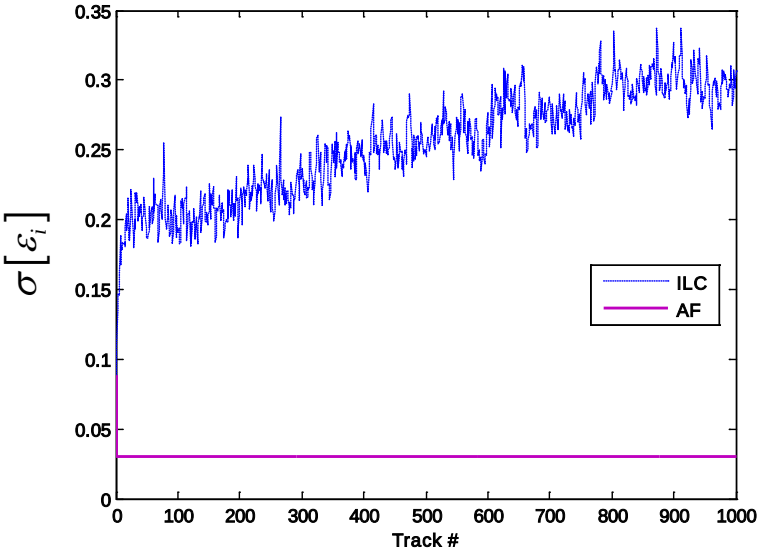

Figure 3.15 Comparison of Circumferential Timing Error ε_i

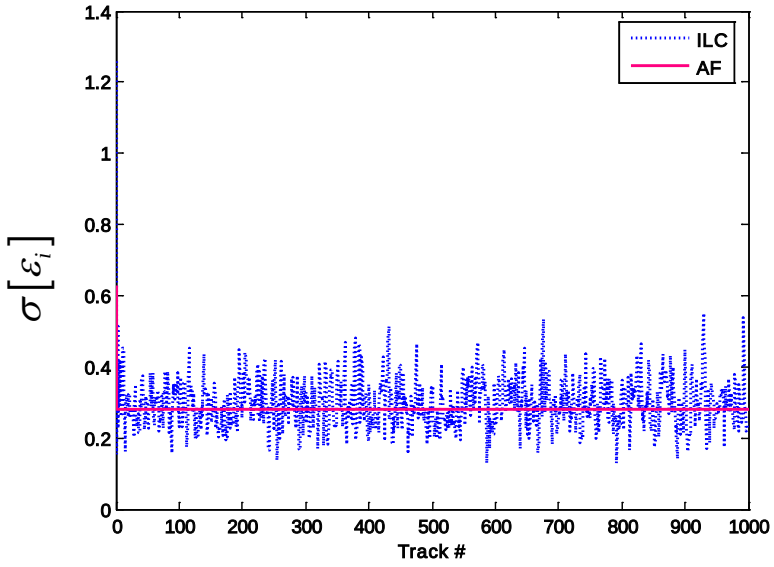

Figure 3.16 Comparison of Radial Timing Error e_i

4 CONCLUSIONS AND CHALLENGES

4.1 Conclusions

The control issues and objectives in SSW servo system have been presented in this report. Effective control schemes were designed for both position control loop and timing control loop.

In the position control loop, two control approaches were proposed: ILC and 2-D control. In ILC control structure, an external correction signal was designed by learning the previous-track errors. The conditions for asymptotic convergence and monotonic convergence were derived. An L_1 optimal control problem was formulated for designing the learning filter. SSW process is then modeled as a 2-D Roesser Model. A 2-D control structure is proposed and designed. The stability and convergence of the corresponding SSW in 2-D model are analyzed and proved. It has been shown that the proposed 2-D control scheme is not only able to guarantee the stability along both the tangential direction and radial direction, but also learn the previous PES information to mitigate the Radial Error Propagation. Simulation results verified that the proposed control system achieves good performance and assures the quality of SSW process.

In the timing control loop, an AFC scheme was proposed to estimate the head phase signal and circumferential timing error. Both the radial timing error information and the circumferential timing error information are used for designing the adaptive filter, which was used in the FXLMS algorithm to ensure minimum closure error in each track and minimum track-to-track timing error propagation. The simulation results showed the effectiveness of the proposed approach.

4.2 Future Challenges

The major challenge for future research is to design effective control algorithms for the SSW process which refers to the prewritten spiral reference. In the spiral SSW process, the quality of SSW is dependant on the accuracy of the spirals. When the spirals are written, due to thermal expansion of the disks and Head Stack Assembly (HSA), some speed errors and positions errors occur in the spirals.

A. Repeatable Phase Error

When the spirals are written, some slow drifts of the spiral start location occur due to thermal expansion, and consequently results in repeatable phase error when the final product servo pattern is written, as shown by the dashed lines in Figure 4.1. Hence, in spiral SSW, we need to contain repeatable phase error and prevent its propagation along radial direction to ensure the performance of SSW process.

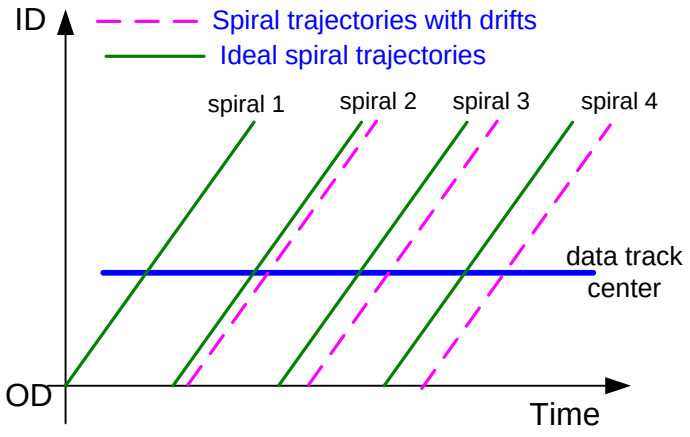

Figure 4.1 Drifts of Spirals

B. Speed Errors in the Spirals

During spiral writing, the external write head is expected to be moved in the radial direction at a constant speed. As illustrated in Figure 4.2, if the speed is faster than the desired constant speed (see the dashed curve), the density of product data tracks will be smaller than the desired track density during SSW (see the dashed line). On the other hand, if the speed is slower (see the dotted curve), it will deteriorate AC track squeeze while the product data track density increases (see the dotted line). Therefore, there is a need to optimize the product data track density to compensate for the spiral density variations due to the speed error during spiral writing. Furthermore, in order to improve the AC track squeeze, effective algorithms for generating PES are necessary.

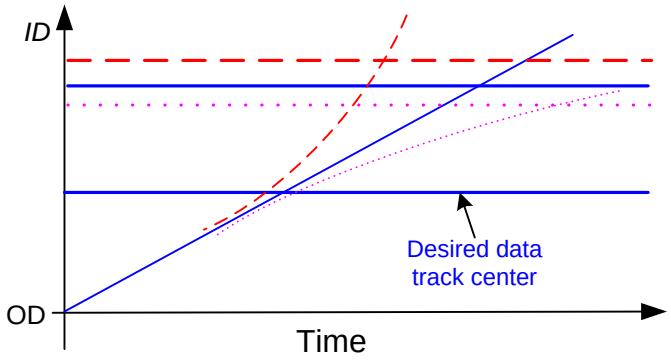

Figure 4.2 Speed Errors in the Spirals

BIBLIOGRAPHY

[1] S-C Wu and M. Tomizuka, "*An Iterative Learning Control Design for Self-Servowriting in Hard Disk Drives*," Proceeding of the 17th IFAC World Congress, July, 2008.

[2] Available: *http://control.ee.ethz.ch/~joloef/wiki/pmwiki.php*.

[3] T. Kaczorek, *Two-dimensional Linear Systems*. New York: Springer-Verlag, 1985.

[4] R. P. Roesser, "*A discrete state-space model for linear image processing*," IEEE Trans. Automatic Control, Vol. AC-20, no. 1 Feb. 1975.

[5] W-S. Lu, E. B. Lee, "*Stability Analysis for two-dimensional systems*," IEEE Trans. Circuits and Systems, Vol. CAS-30, no. 7, pp. 455-461, 1983.

[6] S. Arimoto, S. Kawamura and F. Miyazaki, "*Bettering operation of robots by learning*," J. of Robotic Systems, vol. 1, no. 2, pp. 123-140, 1984.

[7] M. Uchiyama, "*Formulation of high-speed motion pattern of a mechanical arm by trial*," Trans. SICE (Soc. Instrum. Contr. Eng.), vol. 14, no. 6, pp. 706-712 (in Japanese), 1978.